Gas Phase Photocatalytic CO_2 Reduction, "A Brief Overview for Benchmarking"

Shahzad Ali [1,†]**, Monica Claire Flores** [1,†]**, Abdul Razzaq** [2,†]**, Saurav Sorcar** [1]**,**
Chaitanya B. Hiragond [1]**, Hye Rim Kim** [1]**, Young Ho Park** [1]**, Yunju Hwang** [1]**, Hong Soo Kim** [1]**,**
Hwapyong Kim [1]**, Eun Hee Gong** [1]**, Junho Lee** [1]**, Dongyun Kim** [1] **and Su-Il In** [1,*]

[1] Department of Energy Science & Engineering, DGIST, 333 Techno Jungang-daero, Hyeonpung-eup, Dalseong-gun, Daegu 42988, Korea

[2] Department of Chemical Engineering, COMSATS University Islamabad, Lahore Campus, 1.5 KM Defence Road, Off Raiwind Road, Lahore 54000, Pakistan

* Correspondence: insuil@dgist.ac.kr; Tel.: +82-053-785-6417

† These authors contributed equally to this work.

check for
updates

Abstract: Photocatalytic CO_2 reduction is emerging as an affordable route for abating its ever increasing concentration. For commercial scale applications, many constraints are still required to be addressed. A variety of research areas are explored, such as development of photocatalysts and photoreactors, reaction parameters and conditions, to resolve these bottlenecks. In general, the photocatalyst performance is mostly adjudged in terms of its ability to only produce hydrocarbon products, and other vital parameters such as light source, reaction parameters, and type of photoreactors used are not normally given appropriate attention. This makes a comprehensive comparison of photocatalytic performance quite unrealistic. Hence, probing the photocatalytic performance in terms of apparent quantum yield (AQY) with the consideration of certain process and experimental parameters is a more reasonable and prudent approach. The present brief review portrays the importance and impact of aforementioned parameters in the field of gas phase photocatalytic CO_2 reduction.

Keywords: apparent quantum yield; organic contaminations; photocatalyst; solar; CO_2 reduction; photoreactors

1. Introduction

Photocatalytic products, as a consequence of CO_2 photoreduction, are industrially desirable with the additional benefit of normalizing anthropogenic CO_2 [1]. It is inevitable to develop and design efficient photoreactors and optimize the photoreaction conditions in order to scale up the photocatalytic process, all in congruence with synthesis of robust photocatalysts [2]. Although there have been many studies pertaining to the synthesis of stable and efficient photocatalysts, only few studies are dedicated upon reaction engineering so as to ascertain the optimum reaction conditions and photo reactor design [3]. Both of these factors have significant influence on photocatalytic yield. For instance, product yield will be different for photoreactors with batch and continuous flow operation under different conditions of reaction parameters, feed type and concentration ratio, photocatalyst loadings, and sources of irradiation [4,5]. In particular, irradiation sources and its mode of irradiation over the photocatalyst have vital importance. As most of the frequently used photocatalysts are Ultraviolet (UV) light active, irradiation from UV source as compared to solar light will significantly enhance the product yield [6–8]. Further, solar concentrator technology with utilization of Fresnel lens for photocatalyst irradiation leads to enhanced light intensity and photon flux, which in turn renders a significant enhancement in yield of hydrocarbon products [8,9]. Although, most of the photocatalytic

reactions are carried out at room temperature, concentrating solar light will increase the temperature of the system, which will induce the thermal effect that alters the yield [6,7].

Another decisive factor is the exposed area of the photocatalyst to interact with the light irradiations. Even for the different types of photocatalysts, when tested under similar conditions and with yields reported per gram of photocatalyst, a comparison can be misleading because the exposure area, per gram of the photocatalyst, to light will be different for powder catalysts and thin films [10,11]. Moreover, irrespective of photoreaction under standard conditions, yields have been reported in different customary units i.e., ppm cm^{-2} h^{-1}, μmol g^{-1} h^{-1} and μmol cm^{-2} h^{-1} which further complicates the comparison [12–15]. Thus, photocatalysts that are tested under such different conditions and reporting consequent yield in different units lead to ambiguity for fair performance comparison. It is inappropriate to compare the activities of the photocatalysts on the basis of their intrinsic performance without considering effects of optimum conditions and reactor geometries because of these implications.

The aforementioned bottlenecks strongly advocate the necessity for standardized protocols in order to compare the results for photocatalytic CO_2 reduction on equal grounds. Therefore, reporting yields on the basis of photonic efficiency, which incorporates the radiation source and exposure area of the photocatalyst, is an appealing approach [16]. This review specifically focuses on the parameters that influence the actual yield of the photocatalytic CO_2 reduction reactions and outlines the standard testing practices for comparison and evaluation of performance. Moreover, we have calculated the apparent quantum yield (AQY) of different research works, on the basis of data available, for comparing the efficiencies of the photocatalysts.

2. Role of Organic Contaminations

Photocatalysts synthesis predominately involves organic materials as reaction reagents. The residues of such organic materials are not easily removed, even with calcination at higher temperatures. Photocatalytic CO_2 reduction products mainly hydrocarbons, using such catalysts, originate concomitantly from these organic residues and CO_2 as well [1–3]. Thus, yields from such photocatalysts are overestimated when compared to the actual yield originating from photocatalytic CO_2 reduction. However, isotopic labelling by $^{13}CO_2$ is carried out to rule out the possible involvement of these organics in overall photocatalytic yield. To understand the effects of organic contamination, Yang et al. performed Fourier Transform Infrared Spectroscopy (FTIR) investigations for photocatalytic CO_2 reduction over Cu(I)/TiO$_2$ photocatalyst synthesized by two different ways: one with polyethylene glycol (PEG) and another without PEG. The FTIR results showed that Cu(I)/TiO$_2$ with PEG produces more CO (photocatalytic reduction product) as compared to Cu(I)/TiO$_2$ without PEG as shown in Figure 1. This CO originates from organic contaminants even without the introduction of CO_2. The possible mechanism of formation of CO is represented by Equations (1) and (2),

$$CO_2 + C \rightarrow 2CO \tag{1}$$

$$H_2O + C \rightarrow CO + H_2 \tag{2}$$

Calcination at high temperature and illumination under dry He/Ar is incapable of completely wiping out these contaminants [4,5]. However, UV treatment in the presence of H_2O vapors is propitious in removing these contaminants [4]. Furthermore, they extended this study to elucidate the effects of prolonged and repeated pretreatment, for four cycles (7 h each) under He/H_2O, for abolishing organic contaminants. In another study involving the synthesis of Ti-SBA-15 while using P123 (Pluronic acid) and TEOS (Tetraethylorthosilicate) by calcining at 550 °C for 6 h, they revealed the generation of significant amounts of hydrocarbon products (CH$_4$, C$_2$H$_6$, C$_2$H$_4$) under He/H_2O environment. However, the yield of such photocatalytic products was significantly decreased after the first cycle but not diminished completely as shown in Figure 2a–d [5]. Moreover, the control experiments for photocatalytic reduction of CO with H_2O exhibited transition in enhanced selectivity from C$_1$ to C$_2$. Thus, CO produced as

a consequence of organic contamination, as shown in Equations (1) and (2) has profound effects over yield and selectivity of photocatalytic CO_2 reduction [5].
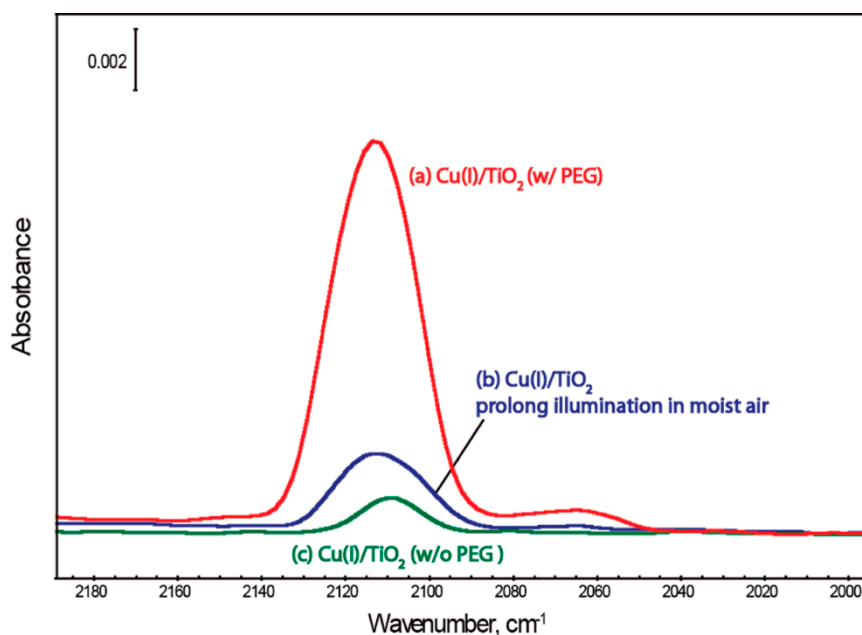

Figure 1. Fourier Transform Infrared Spectroscopy FTIR spectra of Cu(I)/TiO$_2$ preloaded with $^{13}CO_2$ after 80-min illumination. (**a**) fresh Cu(I)/TiO$_2$ (synthesized with PEG), (**b**) Cu(I)/TiO$_2$ cleaned by illumination in humid air for 14 h, and (**c**) reference Cu(I)/TiO$_2$ (synthesized without polyethylene glycol (PEG)), reproduced with permission from reference [4]. Copyright American Chemical Society, 2010.
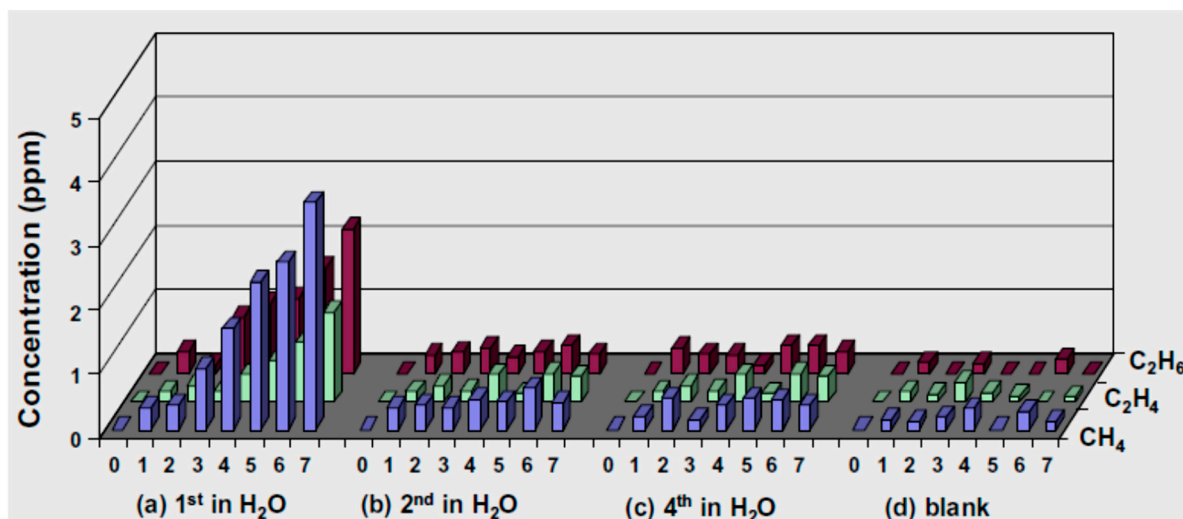

Figure 2. (**a**–**c**) production of CH$_4$, C$_2$H$_6$, and C$_2$H$_4$ over Ti-SBA-15 for four cycles, and (**d**) blank test (without catalyst). After every cycle reactor was evacuated with He/H$_2$O, reproduced with permission from reference [5]. Copyright Elsevier, 2011.

In a similar study by Busser et al., they reported the adsorption of CO_2 over the surface of the photocatalyst during photodeposition of Cu/Cr upon Ga$_2$O$_3$ in the presence of CH$_3$OH [1]. Their study confirmed that the CO_2 originates from photooxidation of methanol as shown in Equation (3).

$$Cu^{2+} + CH_3OH + H_2O \rightarrow Cu^0 + CO_2 + 6H^+ \tag{3}$$
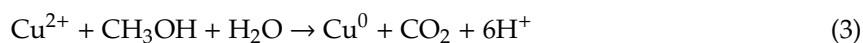
Thus, the assessment of possible contribution of these organic contaminations is indispensable for gauging the actual yield.

3. Flow versus Batch Reactors

Photocatalysts that were tested under different reaction parameters and/or in different reactor geometries can have variability in reaction rate, yield and selectivity [6,7]. Literature suggests variety of reaction conditions and set-ups for photocatalytic CO_2 reduction. Of these conditions, two type of reaction modes are extensively applied in photocatalytic CO_2 reduction: (i) flow reaction system and (ii) batch reaction system [5,9–12]. However, the largely reported use of batch reactors obtains smaller yields of the photocatalytic products. Thus, the activity of the photocatalysts, tested under these different conditions, is imprecise to compare [2,10,13–17].

For batch reactors, it is difficult to understand and control the reaction mechanism and also product composition as well. This is because the products generated in the photocatalytic reaction may get re-adsorb over the surface of the photocatalysts or they can participate in side reactions to yield different products [9,18]. The key limitations of the batch reactor system include an accumulation of the products inside the reactor for a certain defined time which can lead to changes in the concentration of reactants by photocatalytic reactions itself, re-adsorption of the intermediate species or products, and the initiation of side reactions such as hydrogenation or re-oxidation to CO_2. For instance, O_2 that is produced during photocatalytic reduction when adsorbed on the surface of the photocatalyst might compete with CO_2 for electron intake. Thus, batch reactors for CO_2 photoreduction under various experimental conditions make it very difficult to compare the photocatalytic performance and they are not a suitable option for extended time and for industrial scale applications [12]. To resolve such issues, Pipelzadeh et al. designed a pressure swing reactor for facilitated product (CO mainly) desorption. In their configuration, the products were continuously recycled, thus periodic injection/evacuation of gases generated turbulence, which enhanced the CO production yield to 30–80%, depending upon flow rates as shown in Figure 3. Thus the continuous desorption of products is imperative which may surmount mass transfer limitations and the deactivation problems of the photocatalysts [19].

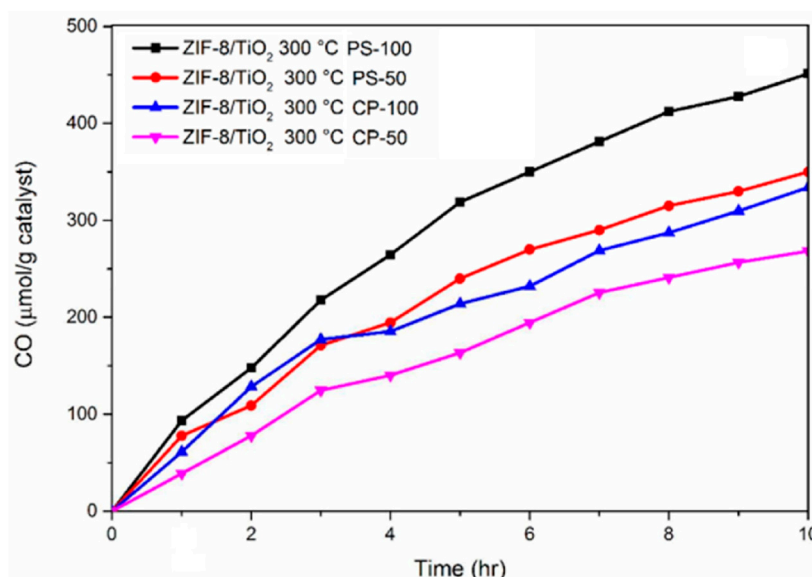**Figure 3.** CO production for ZIF-8/TiO_2 under constant pressure (CP, 5 bar) and pressure swing (PS, 5–3 bar) at flow rates of 50 and 100 mL min^{-1}, reproduced with permission from reference [19]. Copyright Elsevier, 2017.

Contrary to batch reactors the re-adsorption of products and other aforementioned issues can be curtailed in continuous flow reactor system [9]. Despite that, the yield reported is still inadequate

since these types of systems only allow for short residence time of reactants i.e., restricting reactants to make proper contact with photocatalysts. However, better performance can be obtained by optimizing the reaction conditions and using robust photocatalysts [20,21]. In another study, a twin reactor, as shown in Figure 4, was designed to avoid the possible re-oxidation of the photocatalytic products. The photocatalytic CO_2 reduction results revealed that the production of hydrogen and oxygen in separate compartments and then use of as produced hydrogen in CO_2 reduction increased the yield of the products [22].
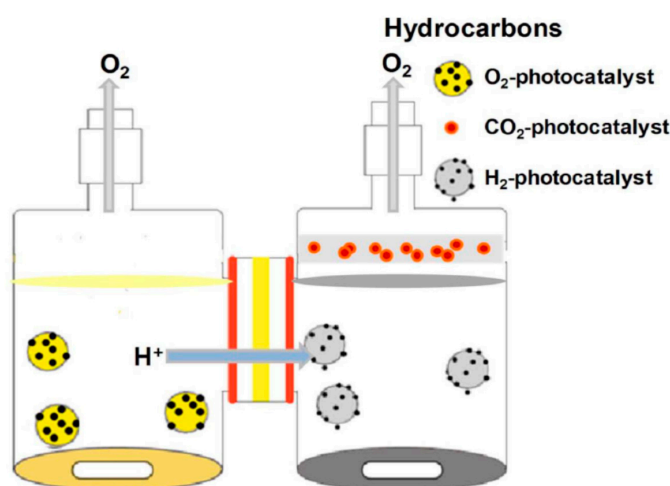

Figure 4. Illustration of twin reactor setup, reproduced with permission from reference [22]. Copyright Elsevier, 2018.

As evident from Table 1, studies by In et al. clearly vindicate the efficacy of transition from batch to continuous flow reactor along with the use of robust photocatalysts. Their well-designed flow reaction system, as shown in Figure 5 consists of a mass flow controller (50 standard cm^3, 20 °C, 1 atm) that regulates the flow of gases, a water bubbler (diameter = 3 cm, length = 15 cm) to maintain the desired humidity, a vacuum pump (pumping speed = 100 L min^{-1}) to obtain high purity conditions by degassing the ultra-sealed photoreactor under a vacuum of 3.5×10^{-3} torr, and a gas chromatography unit for an automatic product intake and analysis (Shimadzu GC-2014, Restek Rt-Q Bond column, internal diameter = 0.53 mm, length = 30 m). Moreover, they used a ceramic porous disc (pore size = 1~1.6 μm) to support the catalyst and a quartz glass (diameter = 5 cm, thickness = 2 mm) to ensure efficient light transfer and the sealing of the reactor. Their research group also optimized the photoreactor dimensions to further improve the reaction process, (as shown in Figure 6a–c).
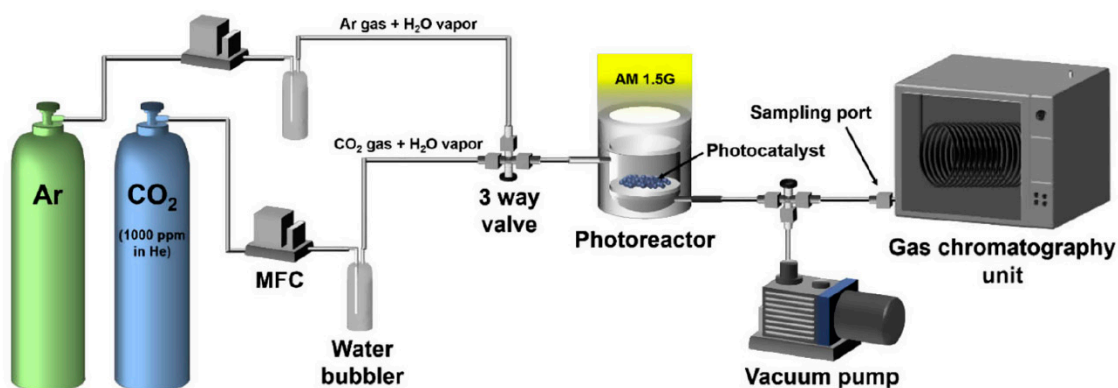

Figure 5. Setup for continuous gas phase photocatalytic CO_2 reduction, reproduced with permission from reference [11]. Copyright Elsevier, 2017.

Table 1. Summary of operating parameters and yields reported by In et al. for photocatalytic CO_2 reduction.

Photocatalyst	Synthesis Method	Pre-Treatment of Reactor	Light Source	Reducing Agent	Reaction Parameters	Reactor	Main Product	AQY (%)
Degussa P25 standard titania [23]	store-bought	purged with high purity CO_2 gas, at least five times	UVP, UVGL-58 lamp with $\lambda = 365$ nm; 1200 μW cm^{-2}	H_2O	50 mg catalyst on a 30 mm diam. glass disk; 15.4 cm^3 reactor; CO_2 flowrate @ 10 cm^3 min^{-1}; 500 μL sample gas extracted; ambient temperature and pressure; 1 h irradiation	Batch reactor	CH$_4$ @ 0.021 μmol g^{-1} h^{-1}	0.0021
CZTS−TiO$_2$ hybrid mesoporous [24]	hot injection and annealing	purged with CO_2 gas (1000 ppm in He) and vacuum	100 W Xe solar simulator with an AM 1.5 filter; 100 mW cm^{-2}	H_2O	50 mg catalyst on a 30 mm diam. glass disk; 15.4 cm^3 reactor; CO_2 flowrate @ 10 cm^3 min^{-1}; 500 μL sample gas extracted; ambient temperature and pressure; 1 h irradiation	Batch reactor	CH$_4$ @ 118.75 ppm g^{-1} h^{-1}	0.0057
CZTS-ZnO nanoparticles [14]	hydrothermal treatment	three times purged with CO_2 gas (1000 ppm in He) and vacuum	100 W Xe solar simulator with an AM 1.5 filter; 100 mW cm^{-2}	H_2O	50 mg catalyst on a 30 mm diam. glass disk; 15.4 cm^3 reactor; CO_2 flowrate @ 10 cm^3 min^{-1}; 500 μL sample gas extracted every 1 h; ambient temperature and pressure; 1 h irradiation	Batch reactor	CH$_4$ @ 0.0954 μmol g^{-1} h^{-1}	0.0128
Cu$_x$O−TiO$_2$ mesoporous p-type/n-type heterojunction material [25]	thermal decomposition then calcination	purged with CO_2 gas (1000 ppm in He) and vacuum	100 W Xe solar simulator with an AM 1.5 filter; 100 mW cm^{-2}	H_2O	50 mg catalyst on a 30 mm diam. glass disk; 15.4 cm^3 reactor; CO_2 flowrate @ 10 cm^3 min^{-1}; 500 μL sample gas extracted; ambient temperature and pressure; 1 h irradiation	Batch reactor	CH$_4$ @ 221.63 ppm g^{-1} h^{-1}	0.0177
Pt-x-RT nanoparticles [15]	magnesio-thermic reduction	five times purged with CO_2 gas (1000 ppm in He) and vacuum	100 W Xe solar simulator with an AM 1.5 filter; 100 mW cm^{-2}	H_2O	70 mg catalyst on a 30 mm diam. glass disk; 15.4 cm^3 reactor; CO_2 flowrate @ 10 cm^3 min^{-1}; 500 μL sample gas extracted; ambient temperature and pressure; 1 h irradiation	Batch reactor	CH$_4$ @ 1.13 μmol g^{-1} h^{-1}	0.1234

Table 1. *Cont.*

| Photocatalyst	Synthesis Method	Pre-Treatment of Reactor	Light Source	Reducing Agent	Reaction Parameters	Reactor	Main Product	AQY (%)
C,N-TNT06 nanotubes [26]	alkaline hydrothermal technique then calcination	purged with CO_2 gas (1000 ppm in He) and vacuum	100 W Xe solar simulator with an AM 1.5 filter; 100 mW cm^{-2}	H_2O	100 mg catalyst on a 30 mm diam. glass disk; 15.4 cm^3 reactor; CO_2 flowrate @ 10 cm^3 min^{-1}; 500 µL sample gas extracted; ambient temperature and pressure; 1 h irradiation	Batch reactor	CH_4 @ 9.75 µmol g^{-1} h^{-1}	1.0532
Pt-XG/RBT nanoparticles [8]	facile vacuum treatment and photodeposition	1 h purging with moist CO_2 gas @ 40 mL min^{-1}	100 W Xe solar simulator with an AM 1.5 filter; 100 mW cm^{-2}	H_2O	40 mg catalyst on a 4.9 cm^2 porous disk; 26.57 cm^3 reactor; CO_2 flowrate @ 1 mL min^{-1}; sample gas analyzed every 30 min; ambient temperature and pressure; 7 h irradiation	Continuous flow reactor	CH_4 @ 37.0 µmol g^{-1} h^{-1} (AQY$_{CH4}$ = 5.248) C_2H_6 @ 11.0 µmol g^{-1} h^{-1} (AQY$_{C2H6}$ = 2.73)	7.978
Pt-BT-X nanoparticles [11]	facile low-temperature synthesis, annealing and photodeposition	1 h purging with moist CO_2 gas @ 40 mL min^{-1}	100 W Xe solar simulator with an AM 1.5 filter; 100 mW cm^{-2}	H_2O	40 mg catalyst on a 4.9 cm^2 porous disk; 26.57 cm^3 reactor; CO_2 flowrate @ 1 mL min^{-1}; sample gas analyzed every 30 min; ambient temperature and pressure; 6 h irradiation	Continuous flow reactor	CH_4 @ 80.35 µmol g^{-1} h^{-1}	12.357
Cu$_{x\%}$–Pt$_{y\%}$–BT nanoparticles [27]	facile low-temperature synthesis, annealing and photodeposition	1 h purging with moist CO_2 gas @ 40 cc min^{-1}	100 W Xe solar simulator with an AM 1.5 filter; 100 mW cm^{-2}	H_2O	40 mg catalyst on a 2.5 cm diam. porous disk; 26.57 cm^3 reactor; CO_2 flowrate @ 1 mL min^{-1}; sample gas analyzed every 30 min; ambient temperature and pressure; 6 h irradiation	Continuous flow reactor	CH_4 @ 3.0 mmol g^{-1} (AQY$_{CH4}$ = 79.14) C_2H_6 @ 0.15 mmol g^{-1} (AQY$_{C2H6}$ = 6.92)	86
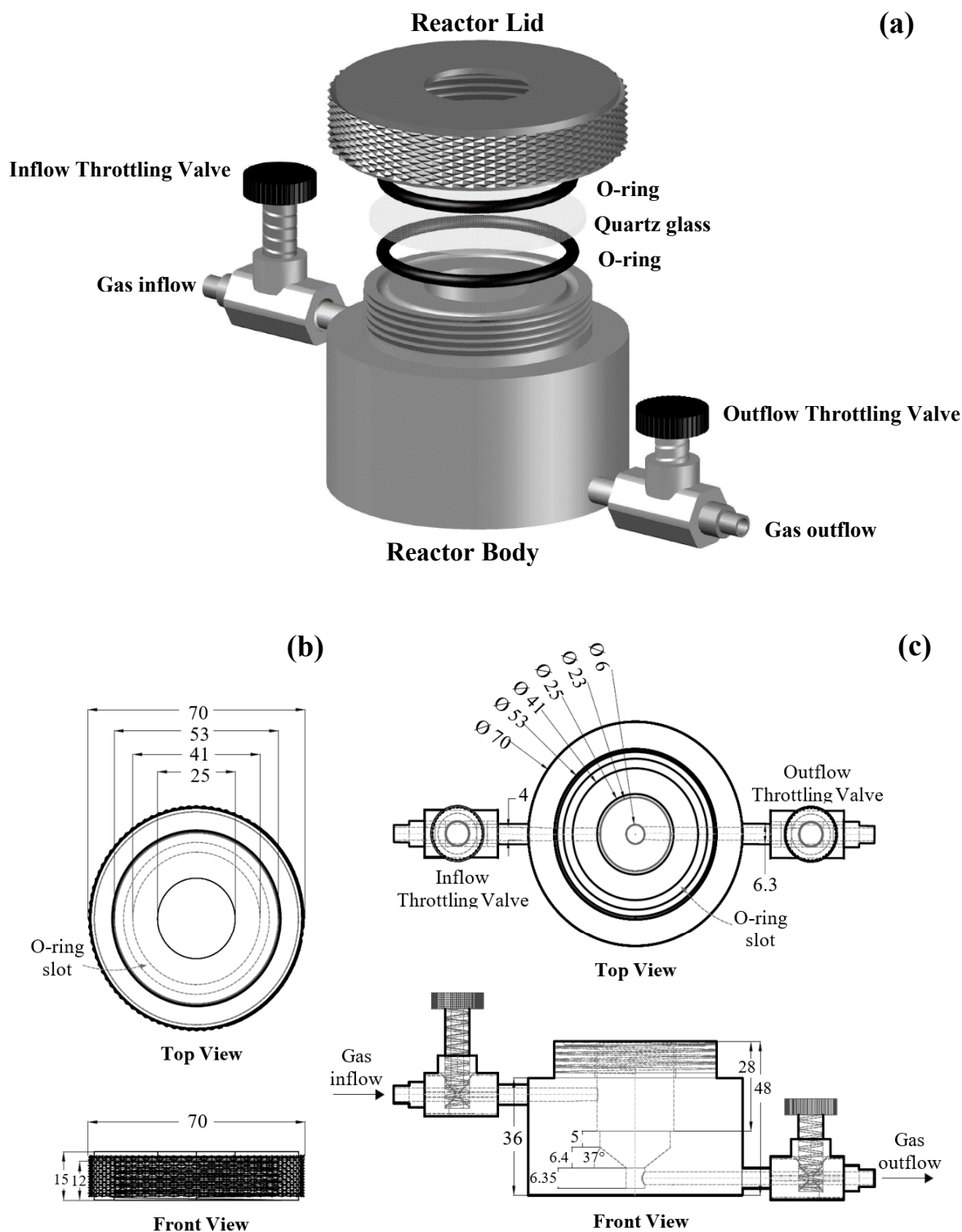
Figure 6. Reactor diagram and its blue prints, (**a**) Complete reactor diagram, (**b**) Lid dimensions, and (**c**) Reactor body dimensions.

4. Reactor Geometry and Catalyst Support

Even the distribution of light over the surface of the photocatalyst is essential in reaping its full potential. In most of the reactor geometries where light impinges over the surface of the photocatalyst, from center or side, a shadow is casted on the opposite side. Consequently, a major portion of the photocatalyst is not activated. The contact of the light and photocatalyst might be enhanced

by fabricating effective reactor geometries to achieve a uniform distribution of light and better photocatalyst dispersion [6,28,29]. Higher dispersion of the photocatalyst results in enhanced contact with reactants, better mass transfer and guarantees the maximum utilization of the light which all eventually translate to higher quantum yield [30]. To achieve this, a variety of approaches are reported in literature including the utilization of different reactor geometries and catalyst supports, as discussed in detail below.

4.1. Monolith Reactor

Tahir et al. studied the effect of photocatalyst dispersion by comparing performance of TiO_2 coated micro channel monolith and cell type support (dispersed as single layer over stainless steel cell). Their study revealed a significant enhancement in CO production by TiO_2 coated monolith as shown in Figure 7. This increment was mainly attributed to a broader exposed photocatalyst surface available for photocatalytic reaction [6]. In their study with gold-indium TiO_2 dispersed over monolith, higher yields were reported particularly formation of C_2 and C_3 products. This enhancement was linked to effective utilization of photons owing to larger illuminated area of monolith [31]. A similar result of enhancement in CO_2 reduction to CH_4 was reported for montmorillonite modified TiO_2 that was loaded over monolith as compared to the bare one [32].However, their performance is still restricted by limited light penetration despite the high flow rates, minimal pressure drop, and large surface area [33–35].
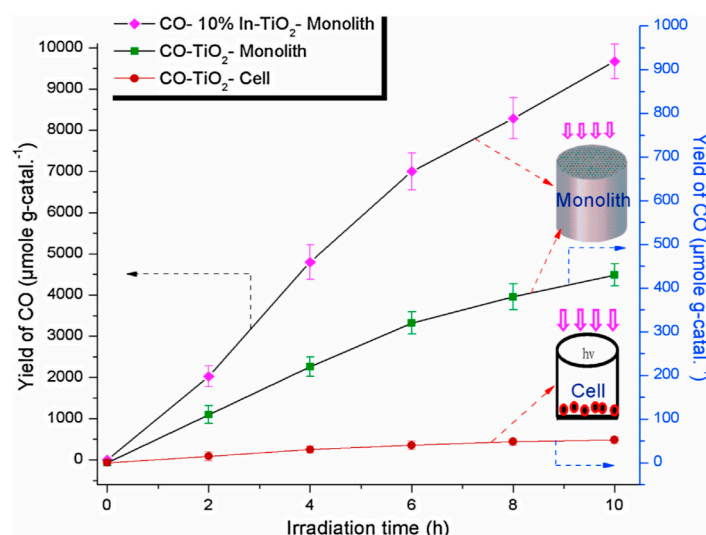

Figure 7. Illustration for comparison of TiO_2 coated on monolith and cell type support, reproduced with permission from reference [6]. Copyright Elsevier, 2013.

4.2. Fiber Optic Reactor

Fiber optic reactors are advantageous when compared to packed bed reactors owing to a better dispersion of photocatalyst and the spreading of light on large surface area [36]. Nguyen et al. compared the yield of the photocatalytic CO_2 reduction carried over the photocatalyst coated on optical fiber and glass plate. Their study demonstrated ~15.2 time enhancement in CH_4 and 11.6 times in C_2H_4 yield, for same amount of photocatalysts. This may be attributed to the synergistic effects of catalyst dispersion and effective light utilization [29]. Wang et al. also carried out CO_2 photoreduction while using fiber optic reactor and they attributed the enhancement in yield to the gradual and uniform distribution of light upon irradiation [37]. Although optical fibers accompany the features of catalyst support and effective light distribution, they are saddled with the constraints of limited utilization of reactor volume and the shorter transportation distance of light from the tip of incidence. They occupy 20–30% of reactor volume, but a limited catalyst coated area restricts the effective use of incident light [33,35,37,38].

4.3. Monolith Fiber Optic Combined Reactor

Ola et al. combined the mutual effects of higher surface area of monolith and effective light distribution of fiber optics to fabricate internally illuminated monolith reactor, and compared the CO_2 reduction performance of this system with slurry reactor. It was found that internal illumination, by optical fibers, of the monolith reactor enhanced quantum efficiency to 23 times owing to the higher surface area of monolith and even the distribution of light by optical fibers [39]. Liou et al. inserted carved polymethylmethacrylate (PMMA) made optical fibers into $NiO/InTaO_4$ coated monolith (honey comb structure) as shown in Figure 8. This reactor when applied for photocatalytic CO_2 reduction enhanced the yield of products (methanol and acetaldehyde). An enhancement in the yield can be attributed to increased surface area, higher photocatalyst loading and effective utilization of the light [35].
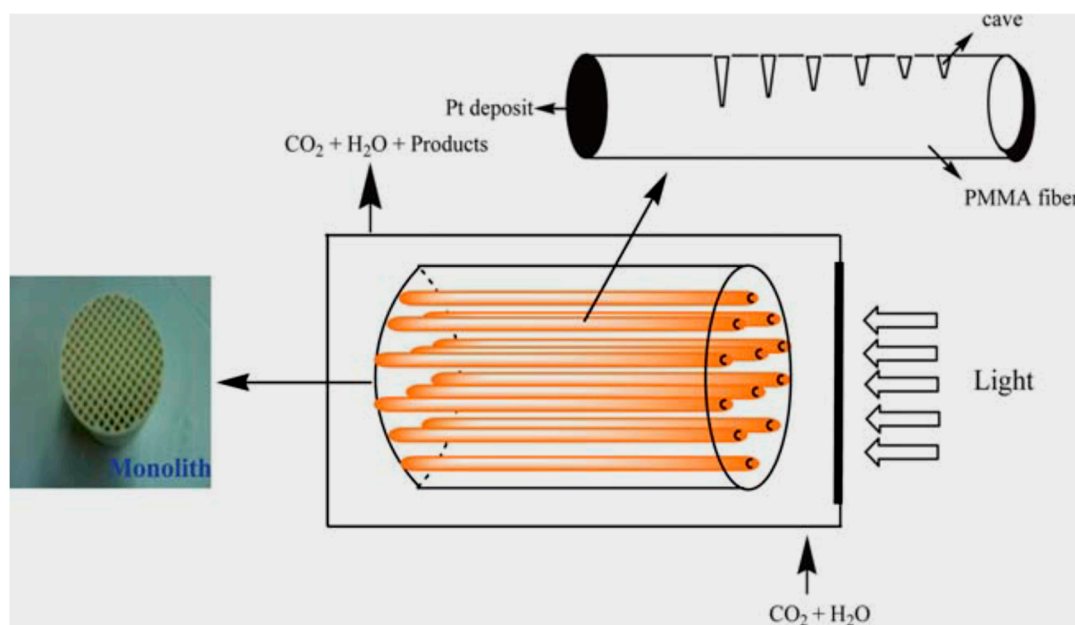

Figure 8. Illustration of monolith fiber optic reactor, reproduced from reference [35] with permission from The Royal Society of Chemistry.

5. Light Irradiations

Light intensity and the type of irradiations are the most influential parameters for photocatalytic CO_2 reduction [40]. Thus, to spur the solar chemical/fuel yielding reactions an effective contact, particularly at the microscopic level, between light and catalyst is imperative. As reported in the literature, a majority of the photocatalysts work efficiently in the UV range thus they are capable of only harnessing a limited range of solar spectrum [41]. To resolve this bottleneck, the modification of semiconductor is carried out for harvesting a wide range of solar spectrum. Other than that, light can be concentrated and channeled to obtain higher photon flux of irradiations [42]. Higher photon flux is not only conducive in propelling apparent quantum efficiency (AQE) but it also shores up the selectivity of multi-electron photoreactions to yield ethane and other long chain solar products. These claims were further vindicated by a study by Nagpal et al. while using TiO_2 and CuInS (copper indium sulfide) nanocrystals as the photocatalyst. An enhanced AQY of 4.3% with a higher ethane selectivity of 70% was observed under concentrated sunlight owing to availability of a higher number of electrons [43]. Han et al. performed CO_2 photoreduction by concentrating light over TiO_2 and Pt/TiO_2. The authors performed CO_2 photoreduction experiments with different concentrating ratio (CR), which is defined as the ratio of concentrated light flux (amount of energy per unit time per unit area) on the photocatalyst surface to the ambient flux (under non-concentrated conditions). The light irradiation is concentrated and varied by changing the distance between the Fresnel lens (placed in

between light source and photocatalyst) and photocatalyst surface, resulting in different light intensities with different light concentrated focal areas. Their study confirmed that the optimum concentration ratio (CR) significantly increased the AQY by 4.0 and 3.17 times for TiO_2 and Pt/TiO_2 respectively [42]. Similar results were reported by Li et al. where photocatalytic CH_4 yield was improved by 29.5 and 6.2 times under optimum CR for untreated and pre-treated samples, respectively [44]. In their other study, they reported that CH_4 yield, for photocatalytic CO_2 reduction, over g-C_3N_4 at CR10 (10 times concentrating the light) was enhanced by factors of ~11.9 and ~16.0 for untreated and pre-treated samples respectively [45]. Tan et al. also reported enhanced AQY up to optimum light intensity but beyond that, it decreases as the number of photons exceeds the requirement for photocatalytic reaction. They also reported that reaction yields were significantly higher for AM 1.5 filter as compared to the UV cut-off filter which could be attributed to higher photon energy for UV leading to the generation of more photogenerated charges [46]. Based on these studies it can be gauged that better contact of light with photocatalyst under optimally concentrated light may lead to an exceptional yield increase.

6. Temperature

Concentrating solar light also increases the temperature depending upon the CR, due to long wavelength irradiations [42,47,48]. Photocatalytic CO_2 reduction at an elevated temperatures is promising as it overcomes the thermal barriers that lead to slow reaction rate and marginal yields [48]. The efficacy of temperature rise for photoreaction can be underscored on the basis of enhanced effective collisions among photogenerated charges and reactants that directly relate to the reaction rate [30,46]. Furthermore, elevated temperature also facilitates the desorption of the products providing the way for the adsorption of the CO_2 on vacant sites leading to increased reaction rate [49,50]. Wang et al. found that production rate almost doubled when the temperature was increased from 25 °C to 75 °C [37]. Desorption of methanol from the photocatalyst surface increases due to increase in temperature, thus providing more active sites for CO_2 photoreduction. The AQY in turn also increased due to more efficient utilization of the incident light and enhanced CO_2 adsorption as result of methanol desorption. However, the reaction temperature should not increase too much as it might also desorb the CO_2 thus decelerating the photoreduction process. Similarly, Guan et al. attained a temperature up to 590 K for photocatalytic reduction of CO_2 and they found temperature rise to be an effective factor for enhancing the yield of solar products [47]. They suggested that such an enhancement was due to the increased collision frequency of photons and diffusion rate of CO_2 towards the surface active sites. Hence the thermal energy along with light irradiation can significantly improve the solar products yield by efficiently overcoming the kinetic barrier for CO_2 photoreduction reactions. In another study Alxneit et al. revealed the rate of CH_4 formation via photocatalytic CO_2 reduction increase when the temperature was increased from 25 to 200 °C. Upon further increasing the temperature, the reaction rate decreased due to desorption of the reactants. However, with the aforementioned temperature range, the reaction rate increases with increasing temperature which indicates the importance of thermal step tending to decrease the surface coverage from intermediate species and products. These results clearly suggest that temperature dependence is one of the pivotal factors that influences the photocatalytic reaction rate and thereof the product yield [48]. In another study, Tahir et al. also confirmed the efficacy of temperature rise in photocatalytic CO_2 reduction for enhanced CO production over In/TiO_2 as shown in the Figure 9 [6]. Such an observation was again explained on the basis of adsorption-desorption phenomenon. Upon increasing the reaction temperature, the mass transfer of CO_2 on the active sites is increased, which leads to increased CO_2 adsorption, resulting in increased reaction rates. They also observed the raising temperature also transformed the product selectivity towards longer chain hydrocarbons. Similarly Zhang et al. reported, when temperature increased from 323 K to 343 K, the yield of the photocatalytic reaction became twice [50]. They also suggested that enhancement in the product yield is due to desorption of products on the photocatalyst surface, providing more chances of collisions between the excited states and adsorbed reactants. Although

raising temperature is an effective strategy to obtain higher yields, different studies suggest that there is always an optimum temperature range to get the best AQY [42].
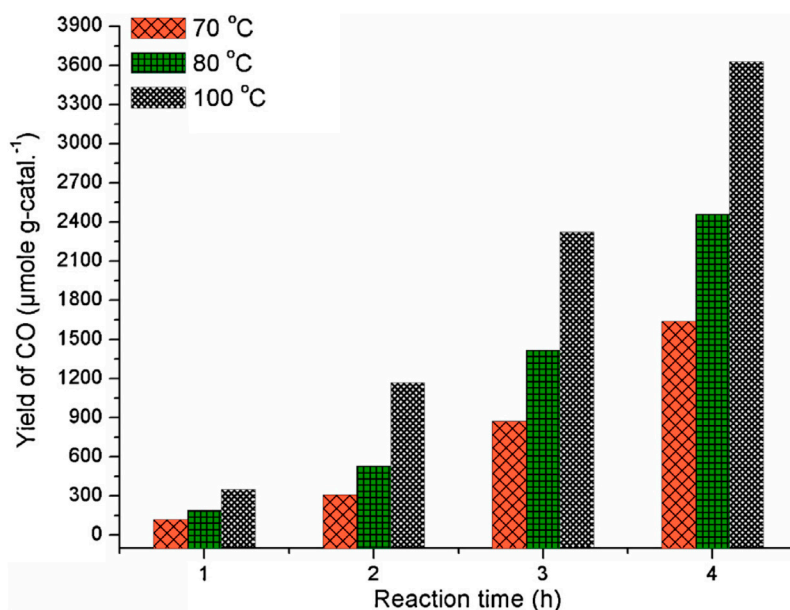

Figure 9. Temperature dependent production of CO, reproduced with permission from reference [6]. Copyright Elsevier, 2013.

7. Effect of H_2O/CO_2 Feed Ratio

An established mixture of water vapors and CO_2 gas (H_2O/CO_2) is considered to be a cost effective and invulnerable feed for photocatalytic reduction into chemicals/fuels. The feed ratio is another crucial factor with a profound impact over reaction rate and product yield. In addition, the affinity of the photocatalyst for H_2O/CO_2 may also lead to well tuning of the product selectivity. Yamashita et al. found highly selective methanol formation over the surface of hydrophilic Ti-Beta(OH) zeolites when compared to conventional Ti-Beta(F) zeolites [51]. Tahir et al. studied the effect of varying H_2O/CO_2 ratio by manipulating the CO_2 flow rates. In their study they reported that at lower concentration of CO_2, water could adsorb over the photocatalyst to react efficiently and give better yields. However, at higher CO_2 concentrations, H_2O has to compete for adsorption which may influence the yield. The same authors also studied the variation in H_2O/CO_2 ratio and its influence on the yield [6]. Zhang et al. also reported similar results mentioning enhancement in yield with increasing H_2O/CO_2 ratio [50]. In another study by Tahir et al., which reports enhancement in CH_4 yield with increasing H_2O/CO_2 ratio. This is attributed to adsorption of excess water molecules over the photocatalyst and resulting in incremented ability to reduce CO_2. Further increase in CO_2 decelerated the yield, shown in Figure 10, due to competition between water and CO_2 molecules on the photocatalyst active sites [30]. As the H_2O/CO_2 feed ratio is increased more water molecules will cover the photocatalyst surface due to hydrophilic nature of the material, which competes with the CO_2 molecules to get adsorb on the photocatalyst active sites during the photoreduction process. Therefore, an optimum feed ratio is required for moderate adsorption of both water and CO_2 molecules which in turn lead to the maximum CH_4 yield. The importance of optimum H_2O/CO_2 ratio was further vindicated by Wu et al. in which they reported optimum H_2O/CO_2 ratio is essential for enhanced yield of methanol [52]. The investigation of Tan et al. also stressed the need for adsorption of optimum number of molecules of CO_2 and H_2O over the catalyst surface to obtain enhanced yields. Moreover it is important to note that, enhanced adsorption of any reactant will certainly hinder the adsorption of others [46]. Thus, a tradeoff should exist between CO_2 and H_2O to mitigate their competitive adsorption over the surface

of the photocatalyst. Thus, due to rivalry in adsorption, an optimum feed ratio is indispensable to get improved yield.
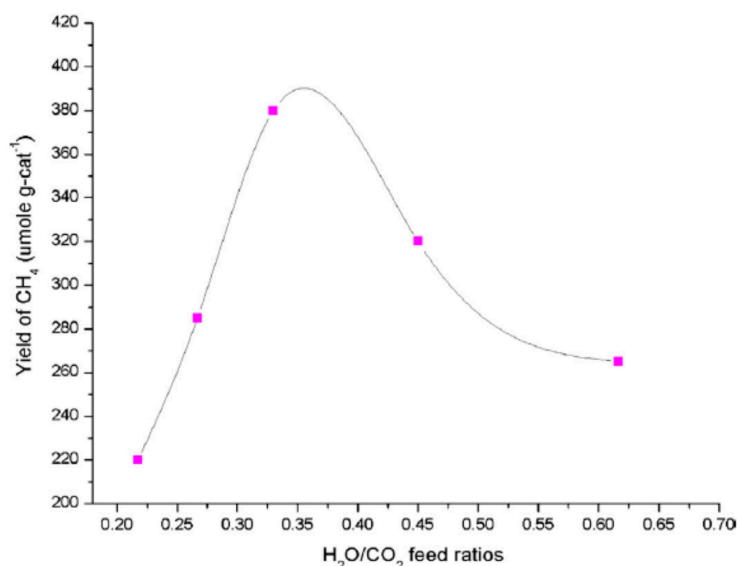

Figure 10. Effect of H_2O/CO_2 ratio over CH_4 yield, reproduced with permission from reference [30]. Copyright Elsevier, 2013.

8. Other Factors

In addition to the above mentioned parameters, there exists several other parameters which also alters the photocatalytic yield. A reported work investigated the performance of photocatalyst in cell type and monolith photoreactor which revealed that broader exposed area of photocatalyst, as for monolith catalyst support, improves the yield (shown in Figure 11). This can be related to enhancement in the illumination area of photocatalyst i.e., exposure of same weight of the catalyst in a larger area [29,30,39,42,53]. In addition to the conditions of high purity, ultra-high vacuum also ensures the absence of external impurities [9]. Moreover, by improving the surface properties like CO_2 adsorption capability, photocatalytic yield can also be improved [44,45,54–58].
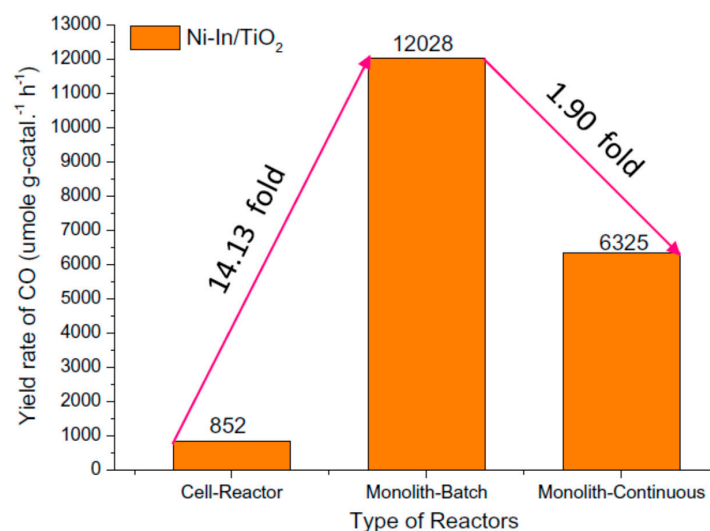

Figure 11. Performance evaluation of cell type and monolith batch/continuous photoreactor for CO_2 photoreduction, reproduced with permission from reference [53]. Copyright Elsevier, 2015.

9. Benchmarking for Performance Evaluation

Based on the above discussion it can be well acknowledged that reactor geometries, reaction parameters, light intensity and wavelength are important parameters that play a pivotal role to control the product yields and selectivity. Thus photocatalysts that were tested under different conditions cannot be compared on equal grounds [42]. Like, Tan et al. reported that a maximum yield of 3.14 μmol g^{-1} was obtained at a light intensity of 177.2 mW cm^{-2} but in terms of AQY, the performance is better at 81 mW cm^{-2}, as shown in Figure 12, for a given amount of photocatalyst [46]. This clearly reveals that although the photocatalyst is producing maximum yield at 177.2 mW cm^{-2} it still underperforms in capitalizing photogenerated charges. Thus, reporting performance of the photocatalytic reaction only on the basis of intrinsic capability of photocatalyst to yield the products is not a rationalized approach. On the contrary, evaluating the performance of the photocatalyst in terms of AQY, which incorporates reactor area, incident and harvested light, can be a more adequate approach [59]. For meaningful performance comparison, AQYs of the different photocatalysts are calculated and presented in Tables 1–3, using Equations (4)–(8) [11,59].

$$\text{AQY (\%)} = \frac{\text{number of reacted electrons}}{\text{effective number of incident photons}} \times 100\%, \tag{4}$$

$$\text{number of reacted electrons} = \left[\begin{array}{c} \text{mole of product} \\ \text{produced in time, t} \end{array}\right] \times \left[\begin{array}{c} \text{number of electrons} \\ \text{required to produce} \\ \text{1 mol of product} \end{array}\right] \times N_A, \tag{5}$$

$$\text{effective number of incident photons} = \frac{\text{light absorbed by the photocatalyst}}{\text{average photon energy}} \times t, \tag{6}$$

$$\text{light absorbed by the photocatalyst} = H \times A, \tag{7}$$

$$\text{average photon energy} = \frac{hc}{\lambda}, \tag{8}$$

where H is the apparent light input (W m^{-2}), A is the geometric irradiation area (m^2), h is Planck's constant (6.626×10^{-34} J·s), c is speed of light (3×10^8 m s^{-1}), λ is the average wavelength of light source (nm) and N$_A$ is Avogadro's number (6.022×10^{23} atoms mol^{-1}).
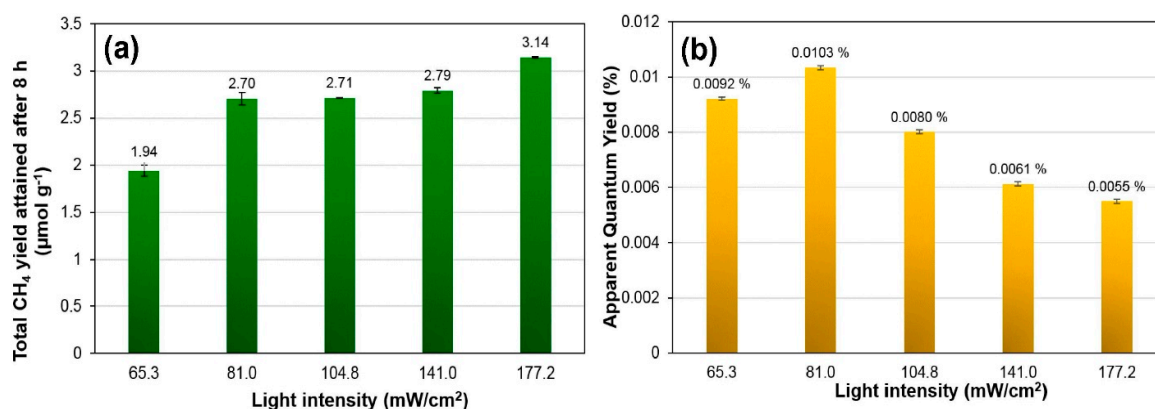

Figure 12. Effect of different light intensities at (**a**) CH$_4$ yield and (**b**) apparent quantum yield(AQY) at variable light intensities, reproduced with permission from reference [46]. Copyright Elsevier, 2016.

Table 2. Summary of operating parameters and yields used by other research works for photocatalytic CO_2 reduction using Batch reactor.

Photocatalyst	Synthesis Method	Pre-Treatment of Reactor	Light Source	Reducing Agent	Reaction Parameters	Reactor	Main Product	AQY (%)
Bi_2WO_6/Au/CdS Z-scheme [61]	bath deposition method	vacuum-treated several times, and then filled with high purity CO_2 gas	300 W Xe lamp ($\lambda > 400$ nm)	0.4 mL of DI water	100 mg catalyst; 230 mL reactor; 1 mL sample gas; ambient pressure; 8 h irradiation	Batch reactor	CH_4 @ ~0.75 μmol g^{-1} h^{-1}	0.012 [b]
rGO-CuO hybrid structure [62]	covalent grafting	purged with nitrogen gas for 15 min then purged with CO_2 for 30 min under continuous stirring	20 W white cold LED flood light (200 < λ < 700 nm); 85 W m^{-2}	mixture of DMF (45 mL) and H_2O (5 mL)	100 mg catalyst; 100 mL reactor; 20 μL total sample gas analyzed; 24 h irradiation	Batch reactor	CH_3OH @ 1282 μmol g^{-1}	0.013 [b,c]
$Cd_{1-x}Zn_xS$ solid solution [63]	two-step self-templated synthesis	purged with argon for 1 h, then 2 mL of deionized water was injected, and purged with ultra-pure CO_2 for 30 min	100 W LED plate with collimating lens; visible light (λ = 450 nm); 285 mW cm^{-2}	2 mL of DI water	45 mg catalyst; 130 cm^3 reactor; 250 μL sample gas extracted every 1 h; 1 atm; 25 °C; 5 h irradiation	Batch reactor	CO @ 2.90 μmol g^{-1} h^{-1} (AQY$_{CO}$ = 0.016) CH_4 @ 0.22 μmol g^{-1} h^{-1} (AQY$_{CH4}$ = 0.005)	0.02 [a]
Co-ZIF-9/TiO_2 nanostructure [64]	in situ growth method	purged with high-purity CO_2 gas	300 W Xe lamp (200 < λ < 900 nm); 494 mW cm^{-2}	3 mL DI water	50 mg catalyst; 390 mL reactor; 0.5 mL sample gas extracted; 70 kPa; 10 h irradiation	Batch reactor with gas circulation system	CO @ 17.58 μmol g^{-1} h^{-1}	0.053 [a]
Pt/TiO_2 mesoporous structure [65]	soft-template method	purged with high purity CO_2 bubbled through DI water for more than 1 h	350 W Xe-lamp with 420 nm cutoff filter; UV light @ 34.8 mW cm^{-2}	H_2O	100 mg catalyst; 159 mL tubular reactor (length: 28 cm, Ø: 3 cm); 60 ± 2 °C; 2 h irradiation	Batch reactor	CH_4 @ 5.7 μmol g^{-1}	0.064 [a]
In_2O_3–C_3N_4 hybrid structure [66]	simple solvothermal method	purged with high-purity CO_2 gas	500 W Xenon lamp; 1200 mW cm^{-2}	0.1 mL ultrapure H_2O	20 mg catalyst; 90 mL reactor; 4 h irradiation	Batch reactor	CH_4 @ 159.2 ppm	0.082 [a]
Pd/(10 wt.% LDH/C_3N_4) hybrid structure [67]	electrostatic interaction	introduction of 200 torr CO_2 into the system	500 W Hg (Xe) lamp without filter	100 mL H_2O	200 mg catalyst; 200 μL sample gas extracted; AQY @ λ = 420 nm; 200 torr; 72 h irradiation	Batch reactor	CH_4 @ 6.5 μmol	0.093 [b]
In/TiO_2-monolith [6]	sol–gel single step method	continuous passing of CO_2, He and H_2O mixture through the reactor for about 1 h	200 W Hg lamp for UV irradiations (λ < 252 nm); 150 mW cm^{-2}	H_2O	50 mg catalyst; 150 cm^3 reactor; 1000 μL sample gas extracted; P$_{CO2}$ = 0.20 bar; P$_{H2O}$ = 0.074 bar; 10 h irradiation	Batch reactor	CO @ 962 μmol g^{-1} h^{-1}	0.10 [b]
TiO_{2-x}/CoO_x hybrid structure [68]	(own method)	blown with CO_2 for 20 min	150 W UV lamp; 20 mW cm^{-2}	2 mL of DI water	50 mg catalyst; 100 mL reactor; 1.01 bar; room temperature; 4 h irradiation	Batch reactor	CO @ 1.247 μmol g^{-1} h^{-1} (AQY$_{CO}$ = 0.0817) CH_4 @ 0.0903 μmol g^{-1} h^{-1} (AQY$_{CH4}$ = 0.0237)	0.105 [a]

Table 2. *Cont.*

Photocatalyst	Synthesis Method	Pre-Treatment of Reactor	Light Source	Reducing Agent	Reaction Parameters	Reactor	Main Product	AQY (%)
Ag-Au/TiO_2 nanowires [69]	facile hydrothermal synthesis	compressed CO_2 and H_2 were continuously passed through the reactor	35 W HID Xe lamp; 20 mW cm^{-2}	H_2	10 mg catalyst; 108 cm^3 reactor; 0.20 bar; 4 h irradiation	Batch reactor	CO @ 1813 µmol g^{-1} h^{-1}	0.1108 [b]
$LaPO_4$–Pt nanorods [70]	hydrothermal method and photo deposition	reactor was evacuated and filled with CO_2 for 1 h with stirring	125 W high-pressure Hg lamp (λ < 365 nm)	70 mL H_2O	50 mg catalyst; 200 mL reactor; 1 atm; 20 °C; 4 h irradiation	Batch reactor	CH_4 @ 0.62 µmol g^{-1}	0.15 [b]
Zn_2GeO_4 micro/mesoporous [71]	simple ion exchange	vacuum-pumped and washed with high purity CO_2 gas	300 W Xe arc lamp (λ = 251 ± 16 nm)	0.5 mL DI water	200 mg catalyst; 360 mL reactor; 0.5 mL sample gas extracted; ambient pressure; 12 h irradiation	Batch reactor	CH_4 @ 9.5 ppm g^{-1} h^{-1}	0.20 [b]
$ZnIn_2S_4$ one-unit-cell atomic layers [72]	(own method)	vacuum-treated three times, then pumped with high-purity CO_2	PLS-SXE300/ 300 UV Xe lamp; 100 mW cm^{-2}	2 mL DI water	100 mg catalyst; atmospheric pressure; 298 ± 0.2 K; 1 h irradiation	Batch reactor	CO @ 33.2 µmol g^{-1} h^{-1}	0.23 [b]
Cu_2O/x% RGO composites [73]	microwave-assisted hydrothermal reaction	CO_2 purged	150 W Xe lamp; 540 µW cm^{-2}	3 mL DI water	500 mg catalyst; 120 mL reactor; sample gas extracted every 30 min; 20 h irradiation	Batch reactor	CO @ 50 ppm g^{-1} h^{-1}	0.34 [b]
Pt/MgAl-LDO/TiO_2 hybrid structure [74]	in-situ deposition, calcination and photo deposition	degassed for 30 min, and then bubbled with CO_2 till the pressure reaches 1 atm	300 W Xe lamp; 1.1 mW cm^2	H_2O	20 mg catalyst; AQY @ λ = 365 nm; 1 atm; 20 °C; 8 h irradiation	Batch reactor	CH_4 @ 0.11 µmol	0.35 [b,c]
LDH/RGO/CN hybrid structure [75]	hydrothermal synthesis and in situ loading	vacuum-treated several times, and then flowed with high purity CO_2 gas	300 W Xe arc lamp; 1.8 mW cm^{-2}	4 mL DI water	50 mg catalyst; 420 mL reactor; 1 mL sample gas extracted; AQY @ λ = 385 nm; ambient pressure; 5 h irradiation	Batch reactor	CO @ 10.11 µmol g^{-1} h^{-1}	0.45 [b]
Cu_2O/WO_3 nanosheets [76]	modified method	vacuum treated, and then purged several times with high purity CO_2 gas	300 W Xenon arc lamp with a UV cutoff filter (λ > 400 nm)	H_2O	85 mg catalyst; 18 h irradiation	Batch reactor	CO @ 0.56 µmol g^{-1} h^{-1}	0.503 [b]
TiO_2 microsphere [77]	sol−gel approach	introduction of pressurized CO_2 @ (50 psi)	40 W Hg UV lamp (λ = 254 nm); 20 mW cm^{-2}	100 µL H_2O	200 mg catalyst; 39 mm diameter and 9 mm depth reactor; 10 mL sample gas extracted; 50 psi; 24 h irradiation	Batch reactor	CO @ 0.56 µmol g^{-1} h^{-1} (AQY$_{CO}$ = 0.204) CH_4 @ 0.94 µmol g^{-1} h^{-1} (AQY$_{CH4}$ = 0.34)	0.54 [b,c]

Table 2. *Cont.*

Photocatalyst	Synthesis Method	Pre-Treatment of Reactor	Light Source	Reducing Agent	Reaction Parameters	Reactor	Main Product	AQY (%)
RGO-CdS nanorod composites [78]	microwave hydrothermal route	degassed with nitrogen for 30 min	300 W Xe arc lamp with a UV-cutoff filter ($\lambda \geq$ 420 nm); 150 mW cm^{-2}	10 mL distilled water	100 mg catalyst; 200 mL reactor; 1 mL sample gas extracted every 1 h; atmospheric pressure and ambient temperature; 3 h irradiation	Batch reactor	CH_4 @ 2.51 μmol g^{-1} h^{-1}	0.80 [b]
HCP-TiO$_2$-FG composite [79]	in situ growth	-	300 W Xe lamp ($\lambda \geq$ 420 nm); 433 mW cm^{-2}	H_2O	20 mg catalyst; standard atmospheric pressure; 5 h irradiation	Batch reactor	CH_4 @ 27.62 μmol g^{-1} h^{-1} (AQY$_{CH4}$ = 1.14) CO @ 21.63 μmol g^{-1} h^{-1} (AQY$_{CO}$ = 0.2227)	1.36 [a]
Co/Pal heterostructure [80]	in situ electrostatic adsorption deposition process	filled with high purity CO_2 gas	300 W Xe lamp	5 mL acetonitrile/H_2O (4:1)	9 mg photosensitizer + 1 mg co-catalyst + 1 mL TEOA; 80 mL reactor; AQY @ λ = 420 nm; 1 atm; 25 °C; 6 h irradiation	Batch reactor	CO @ ~86 μmol	1.38 [b]
CuO−TiO$_2$ hollow microspheres [81]	one-pot template-free synthesis	introduction of pressurized CO_2 @ (50 psi)	40 W Hg UV lamp(λ = 254 nm); 20 mW cm^{-2}	200 μL H_2O	10 mg catalyst; reactor diameter of 39 mm and a depth of 9 mm; 50 psi; 24 h irradiation	Batch reactor	CO @ 14.5 μmol g^{-1} h^{-1} (AQY$_{CO}$ = 1.285) CH_4 @ 2.1 μmol g^{-1} h^{-1} (AQY$_{CH4}$ = 0.747)	2.03 [b]
Pt-TiO$_2$ spheres [77]	microwave-assisted solvothermal method	introduction of pressurized CO_2 @ (50 psi)	40 W Hg UV lamp (λ = 254 nm); 20 mW cm^{-2}	100 μL H_2O	200 mg catalyst; 39 mm diameter and 9 mm depth reactor; 10 mL sample gas extracted; 50 psi; 24 h irradiation	Batch reactor	CO @ 18.9 μmol g^{-1} h^{-1} (AQY$_{CO}$ = 1.632) CH_4 @ 3.6 μmol g^{-1} h^{-1} (AQY$_{CH4}$ = 1.315)	2.95 [b,c]
Pd$_x$Cu$_1$-TiO$_2$ hybrid structures [82]	in situ growth	filled with 0.2 MPa CO_2 for 60 min	300 W Xe lamp (λ < 400 nm); 2 mW cm^{-2}	H_2O	5 mg of TiO$_2$ + 0.01 mmol of metal atoms for catalyst; 100 mL reactor; 0.2 MPa; 2 h irradiation	Batch reactor	CH_4 @ 19.6 μmol g^{-1} h^{-1}	12.53 [a]
In/TiO$_2$ nanoparticles [60]	sol–gel single step method	purged with CO_2 and He for an hour	500 W mercury flash lamp (λ = 365 nm); 40 mW cm^{-2}	H_2O	0.25 mg catalyst; 106 cm^3 reactor; 1000 μL sample gas extracted; 0.20 bars, 373 K; 8 h irradiation	Batch reactor	CH_4 @ 244 μmol g^{-1} h^{-1} (AQY$_{CH4}$ = 42.39) CO @ 81 μmol g^{-1} h^{-1} (AQYCO = 3.52)	45.91 [a]

Table 2. *Cont.*

Photocatalyst	Synthesis Method	Pre-Treatment of Reactor	Light Source	Reducing Agent	Reaction Parameters	Reactor	Main Product	AQY (%)
ZnV_2O_4 microspheres [83]	one-step hydrothermal process	purged with CO_2 gas carrying H_2O for 30 min	35 W HID Xe lamp; 20 mW cm^{-2}	H_2O	100 mg catalyst; CO_2 flowrate @ 20 mL min^{-1}; 108 cm^3 reactor; 0.20 bar; 100 °C; 4 h irradiation	Batch reactor	CO @ 485 µmol g^{-1} h^{-1} (AQY$_{CO}$ = 31.92) CH_3OH @ 100 µmol g^{-1} h^{-1} (AQY$_{CH3OH}$ = 19.75)	51.67 [a]
$NiO/InTaO_4$ monolith coated structure [35]	impregnation method and sol-gel method	purged overnight using a flow of He then switched to pure CO_2 with saturated water vapor for 1 h	300 W Xe arc lamp with AM 1.5 filter; 100 mW cm^{-2}	H_2O	88.7 mg catalyst; 216 cm^3 reactor; 1 bar; 70 °C; 2 h irradiation	-	CH_3OH @ 0.16 µmol g^{-1} h^{-1} (AQY$_{CH3OH}$ = 0.012) CH_3CHO @ 0.3 µmol g^{-1} h^{-1} (AQY$_{CH3CHO}$ = 0.058)	0.07 [b]
MAT nanofibers [84]	(own method)	blown with nitrogen for 30 min	300 W simulated solar Xe arc lamp	H_2O	200 mL reactor; 1 mL sample gas extracted every 1 h; atmospheric pressure and ambient temperature; 3 h irradiation	-	CH_4 @ 0.86 µmol g^{-1} h^{-1}	0.091 [b]
BiOI few-layered nanosheets [85]	(own method)	thoroughly vacuum-treated	300 W high pressure Xe lamp	5 mL H_2SO_4 & 1.712 g $NaHCO_3$	150 mg catalyst; 500 mL reactor; 0.15 mL sample gas extracted; 20 °C AQY @ λ = 420 nm; 4 h irradiation	-	CO @ 0.615 µmol h^{-1} CH_4 @ 0.063 µmol h^{-1}	0.140 [b]
$CdS–WO_3$ heterostructure [86]	simple precipitation method	blown with nitrogen for 30 min	300 W Xe arc lamp with a UV-cutoff filter (λ ≥ 420 nm); 6.0 mW cm^{-2}	H_2O	100 mg catalyst +10 mL of distilled water to form films; 200 mL reactor; 1 mL sample gas extracted every 1 h; AQY @ λ = 420 nm; atmospheric pressure and ambient temperature	-	CH_4 @ 1.02 µmol g^{-1} h^{-1}	0.40 [b]
CeO_x-S/$ZnIn_2S_4$ hybrid structure [87]	one-pot hydrothermal method	introduction of high purity CO_2 gas into the reactor for 3 min	9.0 W (455 nm LEDs)	0.5 mL H_2O	10 mg catalyst; 6.98 mL reactor; 1 bar; below 42 °C; 10 h irradiation	-	CO @ 0.18 mmol g^{-1} h^{-1}	1.34 [b]
Pt/TiO_2 [42]	vacuum impregnation	reactor was cleaned with nitrogen for half an hour then it was replaced and saturated with CO_2 gas for at least 30 min	300 W UV light; 10 mW cm^{-2}	2 mL H_2O	100 mL reactor; sample gas analyzed every 1 h; 0.1 MPa; 7 h irradiation	-	CH_4 @ 20.55 µmol g^{-1}	10.03 [b]

a = AQY computed; b = AQY was computed by authors of the reference paper; c = AQY was computed by authors of the reference paper multiplying it with mass of photocatalyst.

Table 3. Summary of operating parameters used by other research works for photocatalytic CO_2 reduction using Continuous flow reactor.

Photocatalyst	Synthesis Method	Pre-Treatment of Reactor	Light Source	Reducing Agent	Reaction Parameters	Reactor	Main Product	AQY (%)
TiO_2/NRGO-300 nanocomposites [88]	one-step urea-assisted hydrothermal method	purged with CO_2 at 16 mL min^{-1} for 40 min	400 W Xe lamp (250 < λ < 400 nm); 11.5 mW cm^{-2}	H_2O	10 mg catalyst; CO_2 flowrate @ 3 mL min^{-1}; sample gas extracted every 1 h; 8 h irradiation	Continuous flow reactor	CO @ 356.5 μmol g^{-1}	0.0072 [b,c]
5GO–OTiO_2 (UV light) hybrid heterostructure [46]	facile wet chemical impregnation technique	purged with wet CO_2 at 30 mL min^{-1} for 30 min	500 W Xe arc lamp with a UV filter (λ > 400 nm); 81.0 mW cm^{-2}	H_2O	CO_2 flowrate @ 5 mL min^{-1}; Quartz column reactor (ID = 9 mm, OD = 11 mm, length = 250 mm); sample gas extracted every 0.5 h; 1 bar; 25 ± 5 °C; 8 h irradiation	Continuous flow reactor	CH_4 @ 2.7 μmol g^{-1}	0.0103 [b]
TiO_2 nanofibers [89]	sol-gel method and electrospinning technique	firstly, degassed under vacuum and then purged with Ar for 1 h, then fed with CO_2/H_2O mixture in dark for 1 h, then reactor was pressurized and kept at a reaction flow rate of 2 mL min^{-1} for another 1 h.	four 6 W UV lamps (λ$_{max}$ = 365 nm)	H_2O	100 mg catalyst; 190 mL reactor; 7.25 CO_2:H_2O molar ratio; sample gas analyzed every 22 min; 2 bars; 50 °C; 20 h irradiation	Continuous flow reactor	CO @ 203.91 μmol g_{cat}^{-1}	0.04 [b]
Cu/GO-2 hybrid structure [90]	one-pot microwave process	purged with nitrogen gas for 1 h then followed by pure CO_2 for another 1 h	300 W halogen lamp; 100 mW cm^{-2}	H_2O	100 mg catalyst; 300 mL reactor; CO_2 flowrate @ 4 μL/min; 25.0 ± 0.5 °C; 2 h irradiation	Continuous flow reactor	CH_3OH @ 2.94 μmol g^{-1} h^{-1} (AQY$_{CH3OH}$ = 0.0296) CH_3CHO @ 3.88 μmol g^{-1} h^{-1} (AQY$_{CH3CHO}$ = 0.065)	0.095 [a]
G/TiO_2-001/101 nanocomposites [91]	one-pot solvothermal method	purged with the CO_2 + H_2O mixture at 200 mL min^{-1} for 1 h and then reduced to 5 mL min^{-1} for 30 min	300W Xe arc lamp (300 < λ < 400 nm); 20.5 mW cm^{-2}	5 mL DI water	10 mg catalyst; 85 mL reactor; sample gas analyzed every 30 min; atmospheric pressure; 120 °C; 4 h irradiation	Continuous flow reactor	CO @ 70.8 μmol g^{-1} h^{-1}	0.0864 [b,c]
BWO-OV/BiOI binanosheets [92]	simple self-assembly approach	purged with the CO_2/H_2O gas mixture at 50 mL min^{-1} for 30 min	500 W Xenon arc lamp with UV cut-off filter (to remove λ < 400 nm)	H_2O	CO_2 flowrate @ 5 mL min^{-1}; sample gas analyzed every 1 h; atmospheric pressure and ambient temperature; 8 h irradiation	Continuous flow reactor	CO @ 320.19 μmol g^{-1} CH_4 @ 18.32 μmol g^{-1}	0.432 [b]
Pt^{2+}–Pt^0/TiO_2 nanoparticles [93]	sol–gel method	purged with CO_2 + H_2O mixture at 200 mL min^{-1} for 1 h and then at 3 mL min^{-1} for another 30 min.	300 W Xe arc lamp UV light irradiation (320 < λ < 420 nm); 32.5 mW cm^{-2}	H_2O	200 mg catalyst; 85 mL reactor; sample gas extracted every 40 min; 50 °C; 7 h irradiation	Continuous flow reactor	CH_4 @ 264.5 μmol g^{-1} (AQY$_{CH4}$ = 1.35) CO (AQY$_{CO}$ = 0.07)	1.42 [b]
(Pt/TiO_2) @rGO core-shell-structured [94]	hydrothermal method	vacuum-treated, then purged with CO_2 gas @ 50 cm^3 min^{-1} for 30 min	300 W Xe lamp (320 < λ < 780 nm); 80 mW cm^{-2}	2.0 mL H_2O	100 mg catalyst; sample gas extracted every 1 h; 0.1 MPa; 4 °C; 8 h irradiation	Continuous flow reactor	CH_4 @ 41.3 μmol g^{-1} h^{-1}	1.93 [b,c]

Table 3. *Cont.*

Photocatalyst	Synthesis Method	Pre-Treatment of Reactor	Light Source	Reducing Agent	Reaction Parameters	Reactor	Main Product	AQY (%)
NiO/Ni-GR nanoparticles [95]	pyrolysis and incipient wetness impregnation	photoreactor was heated at different temperatures	300 W Xe lamp; 2236 W m^{-2}	H_2	40 mg catalyst; 51 mL reactor; 1.3 bar; 200 °C; 2 h irradiation	Continuous flow reactor	CH$_4$ @ 642 μmol g$_{Ni}$$^{-1}$ h^{-1}	1.98 [b]
Pt-TiO$_2$ nanostructured films [96]	aerosol chemical vapor deposition	purged with CO$_2$ and water vapor at 100 mL min^{-1} for 1 h, and then reduced and maintained at 3 mL min^{-1}	400 W Xe lamp (250 < λ < 388 nm); 19.6 mW cm^{-2}	H_2O	0.7 mg catalyst; atmospheric pressure and room temperature; 5 h irradiation	Continuous flow reactor	CH$_4$ @ 1361 μmol g^{-1} h^{-1} (AQY$_{CH4}$ = 2.33) CO @ 179.34 μmol g^{-1} h^{-1} (AQY$_{CO}$ = 0.077)	2.41 [b,c]

a = AQY computed; b = AQY was computed by authors of the reference paper; c = AQY was computed by authors of the reference paper multiplying it with mass of photocatalyst.

Values for the calculations of AQYs included in this review are given in detail in Supplementary Tables S1 and S2. Moreover, prior to photocatalytic testing under CO_2, repeated photocatalytic reduction tests with H_2O and inert gas can rule out the possible role of organic contamination. Further confirmation of the carbon source of photocatalytic products can be ascertained by an isotopic labeling test while using $^{13}CO_2$. Additionally, optimization of the reaction parameters, condition of high purity and effective photocatalyst and light contact can provide an even better judgment of the performance [1,4,9,60].

10. Conclusions

Photocatalytic CO_2 reduction is a fascinating approach owing to its two-fold benefits of CO_2 abatement and its subsequent conversion to renewable fuels/chemicals. However, optimizing this process has been a challenge for researchers as a variety of process parameters and reaction conditions indistinctly influence the product yield. One parameter is the reaction temperature which by increasing overcomes the kinetic barrier; but on the contrary, excessive temperature might also lead to decomposition. The reactants feed ratio also affects the product yield: at an optimum value, it synergizes the product yield and selectivity but beyond which, the non-stoichiometric ratios of H_2O/CO_2 are competing to get adsorbed on the photocatalyst, resulting in decreased productivity. In addition, optimal light intensity is imperative to produce stoichiometric amount of photogenerated charges for efficient transformation of adsorbed H_2O/CO_2 to solar fuel/chemicals; surplus of these charges, produced at higher light intensities, will recombine and eventually reduce the AQY. Moreover, productivity enhancement also depends on the choice of reactor type: continuous flow reactors have shown potential in overcoming the low yield, re-adsorption, and decomposition of photocatalytic products accustomed to batch reactors. Additionally, the reactor geometry with better light and photocatalyst contact notably affects the production yield. Knowing how these parameters affect the product yield, performance of the photocatalysts tested under different conditions are inappropriate to compare in frequently used customary units i.e., μmol g^{-1} or ppm cm^{-2}. Hence, with the consideration of various process parameters and reaction conditions i.e., reaction temperature, feed ratio, irradiation source, reactor type and geometry, reporting yield of the photocatalysts in terms of AQYs rather than production rate is a more appropriate and pragmatic approach. Additionally, the removal of organic contamination, isotopic labelling, and photocatalytic CO_2 reduction under inert and ultra-sealed condition can provide more realistic assessment of performance.

The overall aim of the present review article is to highlight the influence of key process and reaction parameters on CO_2 photoreduction process to be used for benchmarking. While considering all the aforementioned parameters, a continuous and ultra-sealed gas phase reactor purged under high vacuum with an optimum blend of temperature, feed ratio, and offering larger contact between light and photocatalyst can be an effective approach for achieving maximum yield with the effective utilization of incident photons. Moreover, in order to compare the photocatalytic system performance, a unified parameter should be recognized; reporting yield in terms of AQY standardizes the photocatalytic performance analysis by normalizing the effect of the most influential parameters. Our aforementioned photoreaction setup and studies, well matching with the concluded benchmarking criteria, can be followed for future studies in the field of gas phase CO_2 photoreduction.

Author Contributions: S.-I.I. conceptualized and edited the manuscript, S.A., M.C.F., A.R., S.S., C.B.H., H.R.K., Y.H.P., Y.H., H.S.K., H.K., E.H.G., J.L. and D.K. wrote the manuscript.

References

1. Busser, G.W.; Mei, B.; Pougin, A.; Strunk, J.; Gutkowski, R.; Schuhmann, W.; Willinger, M.; Schlögl, R.; Muhler, M. Photodeposition of Copper and Chromia on Gallium Oxide: The Role of Co-Catalysts in Photocatalytic Water Splitting. *ChemSusChem* **2014**, *7*, 1030–1034. [CrossRef] [PubMed]

2. Razzaq, A.; Grimes, C.A.; In, S.-I. Facile Fabrication of a Noble Metal-free Photocatalyst: TiO_2 Nanotube Arrays Covered with Reduced Graphene Oxide. *Carbon* **2016**, *98*, 537–544. [CrossRef]

3. Shi, R.; Chen, Y. Controlled Formation of Defective Shell on TiO_2 (001) Facets for Enhanced Photocatalytic CO_2 Reduction. *ChemCatChem* **2019**, *11*, 2270–2276. [CrossRef]

4. Yang, C.C.; Yu, Y.H.; Van Der Linden, B.; Wu, J.C.S.; Mul, G. Artificial Photosynthesis over Crystalline TiO_2-Based Catalysts: Fact or Fiction? *J. Am. Chem. Soc.* **2010**, *132*, 8398–8406. [CrossRef] [PubMed]

5. Yang, C.C.; Vernimmen, J.; Meynen, V.; Cool, P.; Mul, G. Mechanistic Study of Hydrocarbon Formation in Photocatalytic CO_2 Reduction over Ti-SBA-15. *J. Catal.* **2011**, *284*, 1–8. [CrossRef]

6. Tahir, M.; Amin, N.S. Photocatalytic CO_2 Reduction and Kinetic Study Over In/TiO_2 Nanoparticles Supported Microchannel Monolith Photoreactor. *Appl. Catal. A Gen.* **2013**, *467*, 483–496. [CrossRef]

7. Delavari, S.; Amin, N.A.S. Photocatalytic Conversion of CO_2 And CH_4 Over Immobilized Titania Nanoparticles Coated on Mesh: Optimization and Kinetic Study. *Appl. Energy* **2016**, *162*, 1171–1185. [CrossRef]

8. Sorcar, S.; Thompson, J.; Hwang, Y.; Park, Y.H.; Majima, T.; Grimes, C.A.; Durrant, J.R.; In, S.-I. High-Rate Solar-Light Photoconversion of CO_2 to Fuel: Controllable Transformation from C_1 to C_2 Products. *Energy Environ. Sci.* **2018**, *11*, 3183–3193. [CrossRef]

9. Dilla, M.; Schlögl, R.; Strunk, J. Photocatalytic CO_2 Reduction under Continuous Flow High-Purity Conditions: Quantitative Evaluation of CH_4 Formation in the Steady-State. *ChemCatChem* **2017**, *9*, 696–704. [CrossRef]

10. Kondratenko, E.V.; Mul, G.; Baltrusaitis, J.; Larrazábal, G.O.; Pérez-Ramírez, J. Status and Perspectives of CO_2 Conversion into Fuels and Chemicals by Catalytic, Photocatalytic and Electrocatalytic Processes. *Energy Environ. Sci.* **2013**, *6*, 3112–3135. [CrossRef]

11. Sorcar, S.; Hwang, Y.; Grimes, C.A.; In, S.-I. Highly Enhanced and Stable Activity of Defect-Induced Titania Nanoparticles for Solar Light-Driven CO_2 Reduction into CH_4. *Mater. Today* **2017**, *20*, 507–515. [CrossRef]

12. Li, Y.; Wang, W.N.; Zhan, Z.; Woo, M.H.; Wu, C.Y.; Biswas, P. Photocatalytic Reduction of CO_2 with H_2O on Mesoporous Silica Supported Cu/Tio_2 Catalysts. *Appl. Catal. B Environ.* **2010**, *100*, 386–392. [CrossRef]

13. Zubair, M.; Kim, H.; Razzaq, A.; Grimes, C.A.; In, S.-I. Solar Spectrum Photocatalytic Conversion of CO_2 to CH_4 Utilizing TiO_2 Nanotube Arrays Embedded with Graphene Quantum Dots. *J. CO_2 Util.* **2018**, *26*, 70–79. [CrossRef]

14. Zubair, M.; Razzaq, A.; Grimes, C.A.; In, S.-I. Cu_2ZnSnS_4 (CZTS)-ZnO: A Noble Metal-Free Hybrid Z-Scheme Photocatalyst For Enhanced Solar-Spectrum Photocatalytic Conversion of CO_2 To CH_4. *J. CO_2 Util.* **2017**, *20*, 301–311. [CrossRef]

15. Razzaq, A.; Sinhamahapatra, A.; Kang, T.H.; Grimes, C.A.; Yu, J.S.; In, S.-I. Efficient Solar Light Photoreduction of CO_2 to Hydrocarbon Fuels Via Magnesiothermally Reduced TiO_2 Photocatalyst. *Appl. Catal. B Environ.* **2017**, *215*, 28–35. [CrossRef]

16. Kim, H.R.; Razzaq, A.; Grimes, C.A.; In, S.-I. Heterojunction pnp Cu_2O/S-TiO_2/CuO: Synthesis and Application to Photocatalytic Conversion of CO_2 to Methane. *J. CO_2 Util.* **2017**, *20*, 91–96. [CrossRef]

17. Parayil, S.K.; Razzaq, A.; In, S.-I. Formation of Titania-Silica Mixed Oxides in Solvent Mixtures and Their Influences for the Photocatalytic CO_2 Conversion to Hydrocarbon. *J. Nanosci. Nanotechnol.* **2015**, *15*, 7285–7292. [CrossRef] [PubMed]

18. In, S.-I.; Nielsen, M.G.; Vesborg, P.C.K.; Hou, Y.; Abrams, B.L.; Henriksen, T.R.; Hansen, O.; Chorkendorff, I. Photocatalytic methane decomposition over vertically aligned transparent TiO_2 nanotube arrays. *Chem. Commun.* **2011**, *47*, 2613–2615. [CrossRef] [PubMed]

19. Pipelzadeh, E.; Rudolph, V.; Hanson, G.; Noble, C.; Wang, L. Applied Catalysis B: Environmental Photoreduction of CO_2 on ZIF-8/TiO_2 nanocomposites in a gaseous photoreactor under pressure swing. *Appl. Catal. B Environ.* **2017**, *218*, 672–678. [CrossRef]

20. Adachi, K.; Ohta, K.; Mizuno, T. Photocatalytic reduction of carbon dioxide to hydrocarbon using copper-loaded titanium dioxide. *Sol. Energy* **1994**, *53*, 187–190. [CrossRef]

21. Teraoka, Y.; Incorporated, F.; Suminoeku, N. Photocatalytic Reduction of CO_2 with H_2O on TiO_2 And Cu/TiO_2 Catalysts. *Res. Chem. Intermed.* **1994**, *20*, 815–823.

22. Xiong, Z.; Kuang, C.C.; Lin, K.Y.; Lei, Z.; Chen, X.; Gong, B.; Yang, J.; Zhao, Y.; Zhang, J.; Xia, B.; et al. Enhanced CO_2 photocatalytic reduction through simultaneously accelerated H_2 evolution and CO_2 hydrogenation in a twin photoreactor. *J. CO_2 Util.* **2018**, *24*, 500–508. [CrossRef]

23. Kim, H.R.; Razzaq, A.; Heo, H.J.; In, S.-I. Photocatalytic conversion of CO_2 into hydrocarbon fuels with standard titania (Degussa P25) using newly installed experimental setup. *Rapid Commun. Photosci.* **2014**, *2*, 64–66. [CrossRef]

24. Kim, K.; Razzaq, A.; Sorcar, S.; Park, Y.; Grimes, C.A.; In, S.-I. Hybrid mesoporous Cu_2ZnSnS_4 (CZTS)–TiO_2 photocatalyst for efficient photocatalytic conversion of CO_2 into CH_4 under solar irradiation. *RSC Adv.* **2016**, *6*, 38964–38971. [CrossRef]

25. Park, S.M.; Razzaq, A.; Park, Y.H.; Sorcar, S.; Park, Y.; Grimes, C.A.; In, S.-I. Hybrid Cu_xO-TiO_2 Heterostructured Composites for Photocatalytic CO_2 Reduction into Methane Using Solar Irradiation: Sunlight into Fuel. *ACS Omega* **2016**, *1*, 868–875. [CrossRef]

26. Parayil, S.K.; Razzaq, A.; Park, S.M.; Kim, H.R.; Grimes, C.A.; In, S.-I. Photocatalytic conversion of CO_2 to hydrocarbon fuel using carbon and nitrogen co-doped sodium titanate nanotubes. *Appl. Catal. A Gen.* **2015**, *498*, 205–213. [CrossRef]

27. Sorcar, S.; Hwang, Y.; Lee, J.; Kim, H.; Grimes, K.M.; Grimes, C.A.; Jung, J.-W.; Cho, C.-H.; Majima, T.; Hoffmann, M.R.; et al. CO_2, Water, And Sunlight to Hydrocarbon Fuels: A Sustained Sunlight to Fuel (Joule-to-Joule) Photoconversion Efficiency of 1%. *Energy Environ. Sci.* **2019**. [CrossRef]

28. Kočí, K.; Reli, M.; Kozák, O.; Lacný, Z.; Plachá, D.; Praus, P.; Obalová, L. Influence of reactor geometry on the yield of CO_2 photocatalytic reduction. *Catal. Today* **2011**, *176*, 212–214. [CrossRef]

29. Nguyen, T.V.; Wu, J.C.S. Photoreduction of CO_2 in an optical-fiber photoreactor: Effects of metals addition and catalyst carrier. *Appl. Catal. A Gen.* **2008**, *335*, 112–120. [CrossRef]

30. Tahir, M.; Amin, N.A.S. Photocatalytic reduction of carbon dioxide with water vapors over montmorillonite modified TiO_2 nanocomposites. *Appl. Catal. B Environ.* **2013**, *142–143*, 512–522. [CrossRef]

31. Tahir, B.; Tahir, M.; Amin, N.S. Gold–indium modified TiO_2 nanocatalysts for photocatalytic CO_2 reduction with H_2 as reductant in a monolith photoreactor. *Appl. Surf. Sci.* **2015**, *338*, 1–14. [CrossRef]

32. Tahir, M.; Tahir, B.; Amin, N.S. Photocatalytic CO_2 reduction by CH_4 over montmorillonite modified TiO_2 nanocomposites in a continuous monolith photoreactor. *Mater. Res. Bull.* **2015**, *63*, 13–23. [CrossRef]

33. Wang, W.; Ku, Y. Photocatalytic degradation of gaseous benzene in air streams by using an optical fiber photoreactor. *J. Photochem. Photobiol. A Chem.* **2003**, *159*, 47–59. [CrossRef]

34. Usubharatana, P.; McMartin, D.; Veawab, A.; Tontiwachwuthikul, P. Photocatalytic process for CO_2 emission reduction from industrial flue gas streams. *Ind. Eng. Chem. Res.* **2006**, *45*, 2558–2568. [CrossRef]

35. Liou, P.Y.; Chen, S.C.; Wu, J.C.S.; Liu, D.; MacKintosh, S.; Maroto-Valer, M.; Linforth, R. Photocatalytic CO_2 reduction using an internally illuminated monolith photoreactor. *Energy Environ. Sci.* **2011**, *4*, 1487–1494. [CrossRef]

36. Wu, J.C.S.; Wu, T.-H.; Chu, T.; Huang, H.; Tsai, D. Application of optical-fiber photoreactor for CO_2 photocatalytic reduction. *Top. Catal.* **2008**, *47*, 131–136. [CrossRef]

37. Wang, Z.Y.; Chou, H.C.; Wu, J.C.S.; Ping Tsai, D.; Mul, G.; Engineering, C. CO_2 photoreduction using NiO/$InTaO_4$ in optical-fiber reactor for renewable energy. *Appl. Catal. A Gen.* **2010**, *380*, 172–177. [CrossRef]

38. Wang, W.; Ku, Y. The light transmission and distribution in an optical fiber coated with TiO_2 particles. *Chemosphere* **2003**, *50*, 999–1006. [CrossRef]

39. Ola, O.; Maroto-Valer, M.; Liu, D.; MacKintosh, S.; Lee, C.W.; Wu, J.C.S. Performance comparison of CO_2 conversion in slurry and monolith photoreactors using Pd and Rh-TiO_2 catalyst under ultraviolet irradiation. *Appl. Catal. B Environ.* **2012**, *126*, 172–179. [CrossRef]

40. Camera-Roda, G.; Santarelli, F.; Martin, C.A. Design of photocatalytic reactors made easy by considering the photons as immaterial reactants. *Sol. Energy* **2005**, *79*, 343–352. [CrossRef]

41. Paulino, P.N.; Salim, V.M.M.; Resende, N.S. Zn-Cu promoted TiO_2 photocatalyst for CO_2 reduction with H_2O under UV light. *Appl. Catal. B Environ.* **2016**, *185*, 362–370. [CrossRef]

42. Han, S.; Chen, Y.; Abanades, S.; Zhang, Z. Improving photoreduction of CO_2 with water to CH_4 in a novel concentrated solar reactor. *J. Energy Chem.* **2017**, *26*, 743–749. [CrossRef]

43. Singh, V.; Beltran, I.J.C.; Ribot, J.C.; Nagpal, P. Photocatalysis deconstructed: Design of a new selective catalyst for artificial photosynthesis. *Nano Lett.* **2014**, *14*, 597–603. [CrossRef] [PubMed]

44. Li, D.; Chen, Y.; Abanades, S.; Zhang, Z. Enhanced activity of TiO_2 by concentrating light for photoreduction of CO_2 with H_2O to CH_4. *Catal. Commun.* **2018**, *113*, 6–9. [CrossRef]

45. Li, D.; Fang, X.; Liu, H.; Lu, H.; Zhang, Z. Photoreduction of CO_2 to CH_4 on g-C_3N_4: The effect of concentrating light and pretreatment. *AIP Conf. Proc.* **2018**, *1971*, 020006.

46. Tan, L.-L.; Ong, W.-J.; Chai, S.-P.; Mohamed, A.R. Photocatalytic reduction of CO_2 with H_2O over graphene oxide-supported oxygen-rich TiO_2 hybrid photocatalyst under visible light irradiation: Process and kinetic studies. *Chem. Eng. J.* **2017**, *308*, 248–255. [CrossRef]

47. Guan, G.; Kida, T.; Yoshida, A. Reduction of carbon dioxide with water under concentrated sunlight using photocatalyst combined with Fe-based catalyst. *Appl. Catal. B Environ.* **2003**, *41*, 387–396. [CrossRef]

48. Saladin, F.; Alxneit, I. Temperature dependence of the photochemical reduction of CO_2 in the presence of H_2O at the solid/gas interface of TiO_2. *J. Chem. Soc. Faraday Trans.* **1997**, *93*, 4159–4163. [CrossRef]

49. Tan, S.S.; Zou, L.; Hu, E. Kinetic modelling for photosynthesis of hydrogen and methane through catalytic reduction of carbon dioxide with water vapour. *Catal. Today* **2008**, *131*, 125–129. [CrossRef]

50. Zhang, Q.H.; Han, W.D.; Hong, Y.J.; Yu, J.G. Photocatalytic reduction of CO_2 with H_2O on Pt-loaded TiO_2 catalyst. *Catal. Today* **2009**, *148*, 335–340. [CrossRef]

51. Yamashita, H.; Ikeue, K.; Takewaki, T.; Anpo, M. In situ XAFS studies on the effects of the hydrophobic-hydrophilic properties of Ti-Beta zeolites in the photocatalytic reduction of CO_2 with H_2O. *Top. Catal.* **2002**, *18*, 95–100. [CrossRef]

52. Wu, J.C.S.; Lin, H.M.; Lai, C.L. Photo reduction of CO_2 to methanol using optical-fiber photoreactor. *Appl. Catal. A Gen.* **2005**, *296*, 194–200. [CrossRef]

53. Tahir, M.; Amin, N.A.S. Performance analysis of nanostructured NiO-In_2O_2/TiO_2 catalyst for CO_2 photoreduction with H_2 in a monolith photoreactor. *Chem. Eng. J.* **2016**, *285*, 635–649. [CrossRef]

54. Ali, S.; Razzaq, A.; In, S.-I. Development of graphene based photocatalysts for CO_2 reduction to C_1 chemicals: A brief overview. *Catal. Today* **2018**, *335*, 39–54. [CrossRef]

55. Hiragond, C.; Ali, S.; Sorcar, S.; In, S.-I. Hierarchical Nanostructured Photocatalysts for CO_2 Photoreduction. *Catalysts* **2019**, *9*, 370. [CrossRef]

56. In, S.-I.; Vaughn, D.D.; Schaak, R.E. Hybrid CuO-$TiO_{2-x}N_x$ Hollow Nanocubes for Photocatalytic Conversion of CO_2 into Methane under Solar Irradiation. *Angew. Chemie Int. Ed.* **2012**, *51*, 3915–3918. [CrossRef]

57. In, S.-I.; Orlov, A.; García, F.; Tikhov, M.; Wright, D.S.; Lambert, R.M. Efficient visible light-active N-doped TiO_2 photocatalysts by a reproducible and controllable synthetic route. *Chem. Commun.* **2006**, 4236–4238. [CrossRef] [PubMed]

58. In, S.-I.; Orlov, A.; Berg, R.; García, F.; Pedrosa-Jimenez, S.; Tikhov, M.S.; Wright, D.S.; Lambert, R.M. Effective visible light-activated B-doped and B, N-codoped TiO_2 photocatalysts. *J. Am. Chem. Soc.* **2007**, *129*, 13790–13791. [CrossRef]

59. Cortes, M.; Hamilton, J.W.J.; Sharma, P.K.; Brown, A.; Nolan, M.; Gray, K.A.; Byrne, J.A. Formal quantum efficiencies for the photocatalytic reduction of CO_2 in a gas phase batch reactor. *Catal. Today* **2019**, *326*, 75–81. [CrossRef]

60. Tahir, M.; Amin, N.S. Indium-doped TiO_2 nanoparticles for photocatalytic CO_2 reduction with H_2O vapors to CH_4. *Appl. Catal. B Environ.* **2015**, *162*, 98–109. [CrossRef]

61. Wang, M.; Han, Q.; Li, L.; Tang, L.; Li, H.; Zhou, Y.; Zou, Z. Construction of an all-solid-state artificial Z-scheme system consisting of Bi_2WO_6/Au/CdS nanostructure for photocatalytic CO_2 reduction into renewable hydrocarbon fuel. *Nanotechnology* **2017**, *28*, 274002. [CrossRef] [PubMed]

62. Gusain, R.; Kumar, P.; Sharma, O.P.; Jain, S.L.; Khatri, O.P. Reduced graphene oxide–CuO nanocomposites for photocatalytic conversion of CO_2 into methanol under visible light irradiation. *Appl. Catal. B Environ.* **2016**, *181*, 352–362. [CrossRef]

63. Kozlova, E.A.; Lyulyukin, M.N.; Markovskaya, D.V.; Selishchev, D.S.; Cherepanova, S.V.; Kozlov, D.V. Synthesis of $Cd_{1-x}Zn_xS$ photocatalysts for gas-phase CO_2 reduction under visible light. *Photochem. Photobiol. Sci.* **2019**, *18*, 871–877. [CrossRef] [PubMed]

64. Yan, S.; Ouyang, S.; Xu, H.; Zhao, M.; Zhang, X.; Ye, J. Co-ZIF-9/TiO_2 nanostructure for superior CO_2 photoreduction activity. *J. Mater. Chem. A* **2016**, *4*, 15126–15133. [CrossRef]

65. Li, X.; Zhuang, Z.; Li, W.; Pan, H. Photocatalytic reduction of CO_2 over noble metal-loaded and nitrogen-doped mesoporous TiO_2. *Appl. Catal. A Gen.* **2012**, *429*, 31–38. [CrossRef]

66. Cao, S.-W.; Liu, X.-F.; Yuan, Y.-P.; Zhang, Z.-Y.; Liao, Y.-S.; Fang, J.; Loo, S.C.J.; Sum, T.C.; Xue, C. Solar-to-fuels conversion over In_2O_3/g-C_3N_4 hybrid photocatalysts. *Appl. Catal. B Environ.* **2014**, *147*, 940–946. [CrossRef]

67. Hong, J.; Zhang, W.; Wang, Y.; Zhou, T.; Xu, R. Photocatalytic Reduction of Carbon Dioxide over Self-Assembled Carbon Nitride and Layered Double Hydroxide: The Role of Carbon Dioxide Enrichment. *ChemCatChem* **2014**, *6*, 2315–2321. [CrossRef]

68. Li, Y.; Wang, C.; Song, M.; Li, D.; Zhang, X.; Liu, Y. TiO_{2-x}/CoO_x photocatalyst sparkles in photothermocatalytic reduction of CO_2 with H_2O steam. *Appl. Catal. B Environ.* **2019**, *243*, 760–770. [CrossRef]

69. Tahir, M.; Tahir, B.; Amin, N.A.S. Synergistic effect in plasmonic Au/Ag alloy NPs co-coated TiO_2 NWs toward visible-light enhanced CO_2 photoreduction to fuels. *Appl. Catal. B Environ.* **2017**, *204*, 548–560. [CrossRef]

70. Pan, B.; Luo, S.; Su, W.; Wang, X. Photocatalytic CO_2 reduction with H_2O over $LaPO_4$ nanorods deposited with Pt cocatalyst. *Appl. Catal. B Environ.* **2015**, *168*, 458–464. [CrossRef]

71. Zhang, N.; Ouyang, S.; Li, P.; Zhang, Y.; Xi, G.; Kako, T.; Ye, J. Ion-exchange synthesis of a micro/mesoporous Zn_2GeO_4 photocatalyst at room temperature for photoreduction of CO_2. *Chem. Commun.* **2011**, *47*, 2041–2043. [CrossRef] [PubMed]

72. Jiao, X.; Chen, Z.; Li, X.; Sun, Y.; Gao, S.; Yan, W.; Wang, C.; Zhang, Q.; Lin, Y.; Luo, Y. Defect-mediated electron–hole separation in one-unit-cell $ZnIn_2S_4$ layers for boosted solar-driven CO_2 reduction. *J. Am. Chem. Soc.* **2017**, *139*, 7586–7594. [CrossRef] [PubMed]

73. An, X.; Li, K.; Tang, J. Cu_2O/reduced graphene oxide composites for the photocatalytic conversion of CO_2. *ChemSusChem* **2014**, *7*, 1086–1093. [CrossRef] [PubMed]

74. Chong, R.; Su, C.; Du, Y.; Fan, Y.; Ling, Z.; Chang, Z.; Li, D. Insights into the role of MgAl layered double oxides interlayer in Pt/TiO_2 toward photocatalytic CO_2 reduction. *J. Catal.* **2018**, *363*, 92–101. [CrossRef]

75. Yang, Y.; Wu, J.; Xiao, T.; Tang, Z.; Shen, J.; Li, H.; Zhou, Y.; Zou, Z. Urchin-like Hierarchical CoZnAl-LDH/RGO/g-C_3N_4 Hybrid as a Z-Scheme Photocatalyst for Efficient and Selective CO_2 Reduction. *Appl. Catal. B Environ.* **2019**, *255*, 117771. [CrossRef]

76. Shi, W.; Guo, X.; Cui, C.; Jiang, K.; Li, Z.; Qu, L.; Wang, J.-C. Controllable synthesis of Cu_2O decorated WO_3 nanosheets with dominant (001) facets for photocatalytic CO_2 reduction under visible-light irradiation. *Appl. Catal. B Environ.* **2019**, *243*, 236–242. [CrossRef]

77. Fang, B.; Bonakdarpour, A.; Reilly, K.; Xing, Y.; Taghipour, F.; Wilkinson, D.P. Large-scale synthesis of TiO_2 microspheres with hierarchical nanostructure for highly efficient photodriven reduction of CO_2 to CH_4. *ACS Appl. Mater. Interfaces* **2014**, *6*, 15488–15498. [CrossRef] [PubMed]

78. Yu, J.; Jin, J.; Cheng, B.; Jaroniec, M. A noble metal-free reduced graphene oxide–CdS nanorod composite for the enhanced visible-light photocatalytic reduction of CO_2 to solar fuel. *J. Mater. Chem. A* **2014**, *2*, 3407–3416. [CrossRef]

79. Wang, S.; Xu, M.; Peng, T.; Zhang, C.; Li, T.; Hussain, I.; Wang, J.; Tan, B. Porous hypercrosslinked polymer-TiO_2-graphene composite photocatalysts for visible-light-driven CO_2 conversion. *Nat. Commun.* **2019**, *10*, 676. [CrossRef]

80. Li, Q.; Lin, F.; Liu, F.; Wang, X. A CO_2 photo-reduction heterogeneous cobalt-based cocatalyst by in-situ electrostatic adsorption deposition. *Chem. Commun.* **2019**, *55*, 3903–3906. [CrossRef]

81. Fang, B.; Xing, Y.; Bonakdarpour, A.; Zhang, S.; Wilkinson, D.P. Hierarchical CuO–TiO_2 hollow microspheres for highly efficient photodriven reduction of CO_2 to CH_4. *ACS Sustain. Chem. Eng.* **2015**, *3*, 2381–2388. [CrossRef]

82. Long, R.; Li, Y.; Liu, Y.; Chen, S.; Zheng, X.; Gao, C.; He, C.; Chen, N.; Qi, Z.; Song, L. Isolation of Cu atoms in Pd lattice: Forming highly selective sites for photocatalytic conversion of CO_2 to CH_4. *J. Am. Chem. Soc.* **2017**, *139*, 4486–4492. [CrossRef] [PubMed]

83. Tahir, M. Hierarchical 3D VO_2/ZnV_2O_4 microspheres as an excellent visible light photocatalyst for CO_2 reduction to solar fuels. *Appl. Surf. Sci.* **2019**, *467*, 1170–1180. [CrossRef]

84. Xu, F.; Meng, K.; Cheng, B.; Yu, J.; Ho, W. Enhanced Photocatalytic Activity and Selectivity for CO_2 Reduction over a TiO_2 Nanofibre Mat Using Ag and MgO as Bi-Cocatalyst. *ChemCatChem* **2019**, *11*, 465–472. [CrossRef]

85. Ye, L.; Wang, H.; Jin, X.; Su, Y.; Wang, D.; Xie, H.; Liu, X.; Liu, X. Synthesis of olive-green few-layered BiOI for efficient photoreduction of CO_2 into solar fuels under visible/near-infrared light. *Sol. Energy Mater. Sol. Cells* **2016**, *144*, 732–739. [CrossRef]

86. Jin, J.; Yu, J.; Guo, D.; Cui, C.; Ho, W. A Hierarchical Z-Scheme CdS–WO_3 Photocatalyst with Enhanced CO_2 Reduction Activity. *Small* **2015**, *11*, 5262–5271. [CrossRef] [PubMed]

87. Hou, T.; Luo, N.; Cui, Y.-T.; Lu, J.; Li, L.; MacArthur, K.E.; Heggen, M.; Chen, R.; Fan, F.; Tian, W. Selective reduction of CO_2 to CO under visible light by controlling coordination structures of $CeOx$-$S/ZnIn_2S_4$ hybrid catalysts. *Appl. Catal. B Environ.* **2019**, *245*, 262–270. [CrossRef]

88. Lin, L.-Y.; Nie, Y.; Kavadiya, S.; Soundappan, T.; Biswas, P. N-doped reduced graphene oxide promoted nano TiO_2 as a bifunctional adsorbent/photocatalyst for CO_2 photoreduction: Effect of N species. *Chem. Eng. J.* **2017**, *316*, 449–460. [CrossRef]

89. Reñones, P.; Moya, A.; Fresno, F.; Collado, L.; Vilatela, J.J.; Víctor, A. Hierarchical TiO_2 nanofibres as photocatalyst for CO_2 reduction: Influence of morphology and phase composition on catalytic activity. *J. CO_2 Util.* **2016**, *15*, 24–31. [CrossRef]

90. Shown, I.; Hsu, H.-C.; Chang, Y.-C.; Lin, C.-H.; Roy, P.K.; Ganguly, A.; Wang, C.-H.; Chang, J.-K.; Wu, C.-I.; Chen, L.-C. Highly efficient visible light photocatalytic reduction of CO_2 to hydrocarbon fuels by Cu-nanoparticle decorated graphene oxide. *Nano Lett.* **2014**, *14*, 6097–6103. [CrossRef]

91. Xiong, Z.; Luo, Y.; Zhao, Y.; Zhang, J.; Zheng, C.; Wu, J.C.S. Synthesis, characterization and enhanced photocatalytic CO_2 reduction activity of graphene supported TiO_2 nanocrystals with coexposed {001} and {101} facets. *Phys. Chem. Chem. Phys.* **2016**, *18*, 13186–13195. [CrossRef] [PubMed]

92. Kong, X.Y.; Lee, W.Q.; Mohamed, A.R.; Chai, S.-P. Effective Steering of Charge Flow through Synergistic Inducing Oxygen Vacancy Defects and pn Heterojunctions in 2D/2D Surface-Engineered $Bi_2WO_{6-x}/BiOI$ Cascade: Towards Superior Photocatalytic CO_2 Reduction Activity. *Chem. Eng. J.* **2019**, *372*, 1183–1193. [CrossRef]

93. Xiong, Z.; Wang, H.; Xu, N.; Li, H.; Fang, B.; Zhao, Y.; Zhang, J.; Zheng, C. Photocatalytic reduction of CO_2 on Pt^{2+}–Pt^0/TiO_2 nanoparticles under UV/Vis light irradiation: A combination of Pt^{2+} doping and Pt nanoparticles deposition. *Int. J. Hydrogen Energy* **2015**, *40*, 10049–10062. [CrossRef]

94. Zhao, Y.; Wei, Y.; Wu, X.; Zheng, H.; Zhao, Z.; Liu, J.; Li, J. Graphene-wrapped Pt/TiO_2 photocatalysts with enhanced photogenerated charges separation and reactant adsorption for high selective photoreduction of CO_2 to CH_4. *Appl. Catal. B Environ.* **2018**, *226*, 360–372. [CrossRef]

95. Mateo, D.; Albero, J.; García, H. Graphene supported NiO/Ni nanoparticles as efficient photocatalyst for gas phase CO_2 reduction with hydrogen. *Appl. Catal. B Environ.* **2018**, *224*, 563–571. [CrossRef]

96. Gangopadhyay, S.; Wang, W.-N.; Biswas, P.; Mukherjee, S.; Ramalingam, B.; An, W.-J.; Niedzwiedzki, D.M. Size and Structure Matter: Enhanced CO_2 Photoreduction Efficiency by Size-Resolved Ultrafine Pt Nanoparticles on TiO_2 Single Crystals. *J. Am. Chem. Soc.* **2012**, *134*, 11276–11281.